

## Response to referees

We thank both referees for constructive comments and suggestions.

Especially the comments on the possible problems arising from the short residence time are very relevant for this study. We believe the improvements we made concerning this topic and other comments significantly add to the quality of the paper.

Since the changes apply to almost every section of the manuscript, we formulate the response as follows:

- The referee comments are shown as blue text, and the corresponding responses as black text.
- The exact changes made to the manuscript are not included in the responses, but instead we attach the new manuscript and supplementary material at the end of the document. The changes are shown as red text.

## Response to Anonymous Referee #1

Simonen et al. present experimental evaluation of the new Tampere Secondary Aerosol Reactor (TSAR). Performance metrics of the TSAR are evaluated against the Potential Aerosol Mass (PAM) oxidation flow reactor: residence time distributions, particle losses, OH exposure, sulfuric acid and toluene SOA yields, and O/C and H/C of toluene SOA. The authors additionally demonstrate the application of the TSAR to resolve changes in the SOA formation potential of car exhaust during dynamometer measurements of a vehicle subjected to a transient driving cycle. The TSAR has potential applications for secondary aerosol formation potential studies of emissions sources. Overall, I was impressed. I would support publication in Atmospheric Measurement Techniques after consideration of my comments below.

1. The authors present evidence that the shorter residence time, higher particle transmission efficiency, and narrower residence time distributions of the TSAR relative to the PAM reactor provide several advantages, especially for transient drive cycle measurements and similar applications. However, in my opinion the short residence time (37 sec) also presents important limitations that are not adequately discussed in the current manuscript. In the absence of significant seed particle surface area, such a short residence time likely limits the condensation of oxidized organic species, to the point that SOA yields that are reported from the TSAR in principle represent lower limits compared SOA yields reported from oxidation flow reactors with longer residence times and/or smog chambers.

For example, the accommodation coefficient ( $\alpha$ ) has been shown to be approximately 0.1 for some oxidized organic vapors that condense to form SOA (e.g. Saleh et al., 2013). To the extent that  $\alpha = 0.1$  is representative of other SOA types, this suggests that the relevant timescales for condensation of oxidized organic vapors ranges from minutes to hours (e.g. Lambe et al., 2015; Seinfeld and Pandis, 1998). This is likely less of an issue in the TSAR for species such as sulfuric acid ( $\alpha \sim 1$ ), which may be why the authors obtain mass closure with sulfuric acid. The following results presented by Simonen et al. further support the hypothesis that condensation of oxidized organic vapors is limited by the short residence time:

- a. Particle size distributions of toluene SOA generated in TSAR and PAM reactor at comparable OH exposure (Fig. 7) show that the mode diameter of SOA particles generated in the TSAR is much smaller than in the PAM reactor (40 nm versus 100

nm).

- b. The maximum toluene SOA yield value obtained in the PAM reactor would increase from ~0.20 to ~0.33 (Fig. 8) if size-dependent particle loss corrections are applied (from statement on Page 14, Line 17, I assume the yields are not currently corrected for losses). This correction is obtained by applying a measured transmission efficiency ~0.6 for 100 nm dioctyl sebacate particles through the PAM reactor (Fig. 2; Lambe et al., 2011). The yield values obtained at other OH exposures would presumably also increase significantly, indicating that toluene SOA yields in the PAM reactor were ~40% or higher than toluene SOA yields measured in the TSAR. Importantly, the mean residence time of the PAM reactor operated in these studies was also significantly higher (~160 sec, as calculated from internal volume of 13.3 L and flow rate 5 LPM).

In my opinion, the authors should add a paragraph near the beginning of the paper that states this up front, and discusses the potential implications of a very short residence time – perhaps at the end of Section 2.1, and elsewhere in the manuscript as appropriate. I think it is also worth attempting to constrain the magnitude of residence-time-limited condensational growth, so that reported TSAR SOA yields obtained with a 37 sec residence time can be corrected (with some uncertainty) to SOA yields that would be obtained with longer condensation times. For example, the authors might consider implementing the “LVOC fate correction” model described in Palm et al. (2016) or something similar to estimate the magnitude of condensable vapors that exit the TSAR before condensing elsewhere.

The limited time for the condensing of oxidized species is now discussed in Sect. 2.5 and the effects are modeled in Sect. 3.4. The effects are also studied in the sections where it is relevant (3.5 and 3.6). Indeed, the LVOC losses are higher in TSAR because of the shorter residence time, especially when the condensational sink is low.

The condensational sink in toluene experiments was high, so that the modeled losses were generally 2 % - 35 %, depending on the value of the accommodation coefficient. Even with the lowest accommodation coefficient (0.1), there was no drastic difference between the losses in PAM and TSAR: at  $2 \times 10^{11} < \text{OH}_{\text{exp}} < 9 \times 10^{11}$  molec.  $\text{cm}^{-3}$  s, the losses in TSAR were ~10 % and in PAM ~7%. At higher and lower  $\text{OH}_{\text{exp}}$  the TSAR losses increase faster than the PAM losses.

The yields were not corrected for the particle losses since the correction for nucleated particles which grow in the PAM is not straightforward. However, we added a paragraph considering the PAM losses, and found that when corrected with the transmission efficiency measured for this particular PAM reactor, the yield is ~19 % higher with the correction (Karjalainen et al., 2016).

2. Page 3, Section 2.1: It may be useful to briefly state why the authors choose to operate the TSAR as an “OFR254” instead of an “OFR185”. I assume that “OFR254” is more practical/safer because the lamps are external to the reactor, and the 185 nm light is not transmitted through the quartz walls of the reactor? Are there additional reasons? Is the UV intensity inside the TSAR varied at all, or is the OH exposure varied by changing the  $\text{O}_3$  and/or  $\text{H}_2\text{O}$  concentrations?

You are right, the OFR254 suits better the TSAR because of the limited transmittance at 185 nm wavelength of the quartz glass. Even if different glass was used, the use of OFR185 mode would require a special ventilation for the TSAR casing to avoid the ozone formation in the room air. This is now clarified in Sect. 2.1. The UV intensity is not varied, and this is clarified in Sect. 2.1 also by describing the lamps as “constant power ozone free low pressure mercury lamps”. However, the

intensity control will be implemented in future to avoid high photon exposure to OH exposure ratio which can cause unwanted photolysis.

3. Page 5, Lines 9-10: The authors state: "the only significant loss of SO<sub>2</sub> in the oxidation reactor is due to the reaction with OH radicals." Was this assumed, or verified experimentally? Was the transmission efficiency of SO<sub>2</sub> measured in the absence of OH? Please clarify.

The SO<sub>2</sub> transmission efficiency was not measured. However, the possible wall loss does not affect the calculation because the SO<sub>2</sub> concentration is always measured after TSAR, with or without UV lights. Thus, the wall loss term in the differential equation cancels out (assuming that the wall loss does not depend on UV lights). This is now clarified in the text.

4. Page 6, Line 4: The authors state: "injecting pressurized air, SO<sub>2</sub>, humidified air and ozone into the TSAR". This is a confusing – isn't the pressurized air also humidified? Figure 1 suggests that some fraction of the carrier gas is sent through a humidifier, another fraction is sent through the ozone generator, and both are mixed prior to entering the residence time chamber.

Yes, a fraction of the carrier gas is sent through a humidifier and the SO<sub>2</sub> is diluted with pressurized air. The sentence was rewritten as follows: "injecting humidified air, ozone and SO<sub>2</sub> diluted with pressurized air".

5. Page 6, Line 27: Consider deleting "which represent atmospheric oxidation" -- in my opinion there are open questions as to how representative all laboratory simulations of atmospheric oxidation chemistry are (flow reactors and smog chambers).

This statement is now removed and discussion about the atmospheric representativeness is added to the Introduction, as recommended by Referee #2.

6. Page 7, Line 9: Please explain why the PAM reactor was run in "OFR185" mode and not also "OFR254" mode to more closely represent the TSAR operating conditions.

We wanted to compare two different systems that produce the same OH exposure to see if TSAR could be used in same applications as PAM, which is usually operated in OFR185 mode at least in engine exhaust measurements (Karjalainen et al., 2016; Timonen et al., 2016; Tkacik et al., 2014). This motivation is now added to the manuscript.

7. Page 8, Line 2: Consider replacing "theoretical residence time" with "calculated mean residence time" or "mean plug-flow residence time", or something similar.

"Theoretical residence time" is now replaced with "mean plug-flow residence time". There was also a mistake in this section: PAM is not twice as big as TSAR, but the PAM volume is approximately four times the volume of TSAR oxidation reactor. This is also corrected in the manuscript.

8. Page 10, Lines 5-9: The added convection caused by UV lamp-induced temperature gradients can be modeled by Taylor dispersion (e.g. Lambe et al., 2011; Huang and Coggon et al., 2016). I suggest applying a Taylor dispersion model to see if this more closely represents the measured residence time distributions that are presented in Figure 3.

According to Huang and Coggon et al. (2016), the Taylor dispersion approximation applies when

$$\tau_{c,cylid} \gg \frac{\tau_{c,D_i}}{3.83^2}$$

where  $\tau_{c,D_i} = \frac{R^2}{D_i}$  and  $\tau_{c,cylid} = \frac{L_{cylid}}{U_{avg}}$ . In TSAR,  $\tau_{c,cylid} = 39 \text{ s}$  and  $\frac{\tau_{c,D_i}}{3.83^2} = 14 \text{ s}$  if  $D_i = 1 \times 10^{-5} \text{ m}^2 \text{ s}^{-1}$ . Thus, we think the use of Taylor dispersion approximation is not justified here.

10. Page 11, Line 9: I did not notice where the output of the UV lamps is discussed. Please report the UV actinic flux that is currently used in the TSAR. This is needed to get at least a qualitative sense of the relative importance of photolysis versus OH oxidation pathways for selected species (e.g. Peng et al., 2016). It should be possible to constrain the UV actinic flux from the measured OH exposures and input ozone and water vapor mixing ratios using the model described in Li et al. (2015) or something similar.

Thank you for this suggestion. We used a photochemical model available in PAM users manual (<https://sites.google.com/site/pamusersmanual/7-pam-photochemistry-model>) and reproduced the measurement results in Sect. 3.3 using the photon flux as one of the fitting parameters. The 254 nm photon flux obtained by fitting was approximately  $1.92 \times 10^{15} \text{ photons cm}^{-2} \text{ s}^{-1}$ .

Based on this photon flux, we also estimate the importance of photolysis in Sect. 3.4.1 as recommended by Referee #2. In addition, the model allows us to estimate better the OH exposure in toluene experiments, and we think this improves Sect. 3.5 significantly (see response to Referee #2, comment 8).

11. Page 11, Section 3.4: The authors might consider combining some of the text from Section 2.5 with Section 3.4, i.e. Page 5 Lines 25-29, Page 6 Lines 1-2 and Lines 10-20 to consolidate the discussion of sulfuric acid yield measurements.

As Referee #2 also pointed out, this section was short and stand-alone. The sulfuric acid measurements are now included in Sect. 3.4.2 to test the LVOC loss model validity.

12. Page 11, Section 3.5: The authors might consider combining some of the text from Section 2.6 (Page 6, Lines 22-30) with Section 3.5.

The beginning of Sect. 3.5 was quite abrupt, and this is corrected now by adding the following sentence at the beginning of Sect. 3.5: "The SOA formation studies were conducted as described in Sect. 2.6."

13. Page 12, Lines 5-7: This argument is speculative and not supported by the measurements. If it were true that "the PAM always outputs SOA with both high  $\text{OH}_{\text{exp}}$  and low  $\text{OH}_{\text{exp}}$ , [thereby reducing] the sensitivity to  $\text{OH}_{\text{exp}}$ ", I would argue that the range of O/C and H/C of PAM-generated toluene SOA should also be narrower than in the TSAR. Figures 9 and 10 show that this is not the case – the range of O/C and H/C is similar in both reactors. I would consider deleting this statement. A more plausible argument, in my opinion, is that the residence-time-limited condensation of oxidized vapors in the TSAR (mean residence time = 37 sec) compared to the PAM reactor (mean residence time ~ 160 sec) results in higher sensitivity to changes in yields of condensable species at the lowest and highest OH exposures that were studied.

We agree that this argument was not supported by the O/C and H/C measurements. After estimating the OH exposure by using the photochemical model, the difference in TSAR and PAM yields is not

anymore so big. There is a difference now only at low OH exposures, but the uncertainty of PAM yields in those cases is very high. Thus, the speculation of PAM OH exposure distribution was removed.

14. Page 12, Line 29 – Page 13, Line 5: Here, it may be useful to know the UV actinic flux in both reactors (see Comment #9). For example, at  $\text{OH}_{\text{exp}} \sim 1.3 \times 10^{12} \text{ molec cm}^{-3} \text{ s}$ , if “F254/OHexp” (as defined by Peng et al., 2016) is significantly different in the TSAR and in the PAM reactor, one might hypothesize that direct UV photolysis of the SOA is more important in one system than the other, and perhaps this is correlated with the observation that  $\text{Osc} \sim 1.1$  in the TSAR and  $\text{Osc} \sim 0.6$  in the PAM reactor (Fig. 10). It is hard to tell without knowledge of the actinic fluxes in both reactors. It may also be useful to add error bars to represent the approximate uncertainties in OH exposure in both systems.

After estimating the OH exposure by using the photochemical model, the difference in TSAR and PAM  $\text{Osc}$  is not as high as before, even though the trend seems to be different between these reactors. However, after applying the error bars arising from the uncertainty of the model, we cannot say whether the difference in trends is real. The error bars for OH exposure are now added to this figure and also to the yield and O/C-H/C figure (Figs. 10,11 and 12 in the new manuscript).

15. Page 9, Section 2.7, Lines 4-6 and Pages 15-16, Section 3.6.2: In Section 2.7, the authors state: “the amount of secondary aerosol mass produced in the TSAR was determined by subtracting the primary mass from the mass measured when using the TSAR.” The absolute secondary-to-primary aerosol mass enhancement is actually never discussed. I think it would be useful to show time series of the primary mass concentration and the secondary-to-primary emission ratio in Figure 13 (perhaps as additional subpanels), discuss in Section 3.6.2, and briefly compare with results from relevant literature studies such as Platt et al. (2013), Tkacik et al. (2014) and Karjalainen et al. (2016).

## References

R. Saleh, N. M. Donahue, and Robinson, A. L.: Time scales for gas-particle partitioning equilibration of secondary organic aerosol formed from  $\alpha$ -pinene ozonolysis, *Environ. Sci. Technol.*, 47, 5588–5594, 2013.

B.B. Palm, P. Campuzano-Jost, A.M. Ortega, D.A. Day, L. Kaser, W. Jud, T. Karl, A. Hansel, J.F. Hunter, E.S. Cross, J.H. Kroll, A. Turnipseed, Z. Peng, W.H. Brune, and J.L. Jimenez. In situ secondary organic aerosol formation from ambient pine forest air using an oxidation flow reactor. *Atmospheric Chemistry and Physics*, *Atmos. Chem. Phys.*, 16, 2943-2970, doi:10.5194/acp-16-2943-2016, 2016. Source code available for download at <https://sites.google.com/site/pamwiki/hardware/estimation-equations>.

Y. Huang, M. M. Coggon, R. Zhao, H. Lignell, M. U. Bauer, R. C. Flagan, and J. H. Seinfeld. The Caltech Photooxidation Flow Tube Reactor – I : Design and Fluid Dynamics. *Atmos. Meas. Tech. Discuss.*, doi:10.5194/amt-2016-282, 2016.

The primary mass and the secondary-to-primary emission ratio are now shown in Fig. 15. The emission factor for the secondary aerosol potential is approximately 25 times the primary mass emission factor. The emission factor is compared with the results from Platt et al. (2013) and Karjalainen et al. (2016), even though the results are not directly comparable since we measured a pre-warm engine as opposed to cold start used by Platt et al. (2013) and Karjalainen et al. (2016). The comparison is

difficult also because the OH exposure in TSAR in this experiment is unknown. Also the comparison to the time-series of secondary aerosol formation measured by Karjalainen et al. (2016) is now carried out.

## Response to Anonymous Referee #2

### General comments:

The manuscript by Simonen et al., describes a new oxidation flow reactor designed to achieve shorter residence time relative to the potential aerosol mass (PAM) reactor. The aim of the new reactor is to provide a method of capturing SOA formation during studies of rapidly changing emission sources (e.g. combustion emissions). Although the subject of the manuscript is appropriate for publication in *Atmospheric Measurement Techniques*, the manuscript in its current state reads more like a technical report at certain parts and lacks sufficient discussion in many places. Most importantly, the manuscript does not contain sufficient emphasis on the atmospheric applicability or relevance in several places. In general, the use of such methodology for studying SOA formation has some benefit if results are not over-interpreted, and used for comparative purposes or during screening experiments to quantify the “potential” SOA formation of a given source or precursor. This is because the methodology is fundamentally limited in terms of its ability to reproduce tropospheric conditions due to unrealistic partitioning behaviour at elevated supersaturation of oxidation products, high OH exposure over a very short period of time and complex OH vs non-OH chemistry resulting from high photon flux at non-tropospheric wavelengths, especially for mixtures of high OH reactivity. Consequently, results of such experiments must not be over-interpreted or used in absolute term. It is recommended that the authors address the general and specific comments adequately before the manuscript is considered for publication.

The discussion in the manuscript is now extended by considering the atmospheric applicability in the Introduction and by considering the effects caused by the short residence time and photolysis in new sections (*2.5 Estimating vapor losses and photolysis* and *3.4 Vapor losses and photolysis in TSAR*). The results from these sections are also applied to Sect. 3.5 and 3.6.

We agree that the flow reactors do not reproduce tropospheric conditions and that their best application is comparative measurements, such as Timonen et al. (2016) where the effect of fuel ethanol content on the exhaust SOA potential was studied using a PAM reactor. However, there is no method that could fully reproduce the conditions in the atmosphere, but still estimations are needed e.g. for emission inventories. Thus, we think also absolute values should be published in similar way as when using smog chambers (e.g. Gordon et al., 2014; Nordin et al., 2013; Platt et al., 2013). This allows comparison of the values also between studies (when the oxidation conditions are comparable). In any case, an adequate error analysis and analysis on atmospheric applicability must be done. This discussion is now added to Introduction and Sect. 2.5 and 3.4.

### Specific comments:

1) In the abstract, the statement about long and short residence times of different reactors should be qualified by adding typical times to provide the reader with an idea about the main

difference between existing techniques and the new TSAR reactor. The abstract should also contain more details about the main modification of the reactor design, which enables the operation at higher time resolution compared to the PAM reactor (e.g. volume, flow rate).

The typical times are now added to the abstract, and also the main difference that enables the higher time resolution compared to the PAM (smaller radius and consequently smaller volume).

2) The introduction should include more critical evaluation of the limitations of existing reactors and chambers with regards to the ability to measure transients and provide typical examples of the residence times of the various reactors mentioned in order to make a case for the need of the new reactor being described in this manuscript.

The motivation for developing TSAR is now clarified in the introduction. We also added discussion about micro smog chamber (MSC, Keller and Burtscher, 2012) which has even shorter residence time than TSAR. In the introduction we discuss why a compromise between PAM and MSC is needed.

3) Page 4, line 1-2: The O<sub>3</sub> needed for this reaction chain is mixed with the sample prior to the residence time chamber. This has an implication on experiments where some of the VOCs react with ozone (e.g. alkenes and biogenic compounds). This should be stated and clarified with discussion of how it would or wouldn't be possible to separate such an effect from that of OH chemistry especially for mixtures of complex composition (i.e. real emissions). The authors touch on this effect later in the manuscript when comparing the oxidation state of SOA produced by the TSAR and PAM reactors (page 12, line 26-27), which emphasise the importance of characterising this aspect of the reactor.

This effect was already mentioned very shortly at the end of Sect. 3.5.1 (p.13, line 20-23 in original manuscript). The discussion is now extended at the end of Sect. 3.5.1 (p. 21, line 10-17). The main application of TSAR is to sample vehicular emissions, and thus the ozone reactive biogenic VOCs are not of concern here. SOA precursors in vehicle emissions are dominated by (non-alkene) compounds that are unreactive toward ozone (Gentner et al., 2012; Tkacik et al., 2014).

It is not possible to fully separate the effect of the initial ozone chemistry on the OH chemistry in the reactor. However, it is possible to measure the SOA formation caused by ozone only by mixing the ozone with the sample with UV lamps turned off.

4) Page 6, line 19-20: Although the authors have shown that the assumption that sulfuric acid losses to the reactor wall are negligible, it is not clear whether this is meant to suggest that such assumption would also hold for oxidation products of organic compounds, which have a wider range of volatility distribution. This should be discussed in the manuscript as it represents a limitation on the ability to quantify SOA yield. On a related note, the sulfuric acid yield section (3.4) is too short to stand alone as it is. The discussion need to be expanded to address this comment.

This is an important aspect that was pointed out by Referee #1, too. The losses of organic compounds are now discussed in Sect. 2.5 and Sect. 3.4. As a result, the sulfuric acid yield section is not stand-alone anymore. According to the model described in Sect. 2.5, the losses of low-volatility organics in toluene yield measurements (Sect. 3.5) in the TSAR are in similar level as in the PAM.

5) Page 7, line 9: It is not clear why the authors did not use the PAM reactor in the OFR254 mode given intended purpose of comparing the results with TSAR which uses a 254nm light source. This should be explained and justified. In addition, the manuscript provides no discussion of the potential effect of the different light sources on the non-OH chemistry in the reactors. The authors should include such discussion in the manuscript in the context of the work published by Peng et al., (2016) quantifying the extent of OH vs. non-OH chemistry according to the conditions applied in the reactor. It is important to understand the role of water mixing ratio, photon flux and external OH reactivity in the experiments on non-OH chemistry (photolysis) in order to establish the atmospheric relevance of the experiments.

See response to Referee #1 (comment 6) concerning the choice of OFR185 for the PAM.

The photolysis is now discussed in sections 2.5 and 3.4 by referring to results in Peng et al. (2016).

6) Page 11, line 21: What is the background mass of the TSAR? How variable is it depending on OH and humidity conditions? Is this characterised and corrected for on a regular basis? More discussion of this should be included.

The background mass is not a feature of the TSAR, but appears also in the PAM and results from the oxidation of the impurities in the dilution air. The dilution air should be cleaned as well as possible to avoid this artefact (this applies to smog chamber experiments as well). The purity of the air is always checked by oxidizing the pressurized air and measuring the mass formed. We expect the dependence on OH exposure and humidity is similar to that of secondary aerosol formation in general. This discussion and the values for the background mass are now added to Sect. 3.5 (p. 18, line 14-17 in the new manuscript).

7) Page 11, line 25-28: More discussion is needed for the apparent link between shorter residence time and the smaller size distribution produced in the TSAR experiment. The potential implication of such phenomena on the produced SOA particles and their properties needs to also be discussed.

In Sect. 3.5, the SOA mass is formed via nucleation and condensation. In TSAR, the oxidation is faster, which leads to higher concentrations of low-volatility compounds. Thus, the ratio of nucleation rate to condensation rate may be higher in the TSAR than in the PAM (Eq. (5) in the new manuscript), which results in smaller particles (but higher concentration) than in the PAM. The modeling of nucleation is complicated, so the validity of this speculation remains a future task. The properties of the SOA particles are expected to be similar based on the results in Sect. 3.5.

The effect of short residence time in general is now discussed in Sect. 2.5 and 3.4, and the discussion in Sect. 3.5 is also extended (p. 18 line 19-26 in the new manuscript).

8) Page 12, line 1-2: How representative is the off-line OH exposure calibration of the actual reported OH exposure in a more complex VOC mixture such that found in the Toluene SOA experiment or other VOC mixtures with different OH reactivates? This is likely to be a source of significant uncertainty in the determination of OH exposure and it is not discussed adequately in the manuscript.

This is a good point. The off-line OH exposure is only the upper limit for the OH exposure in the toluene experiment, since the OH reactivity in the toluene sample is higher than in the off-line calibrations (Li et al., 2015; Peng et al., 2015). We improved the estimation of OH exposure in the toluene experiment by using a photochemical model (see response to Referee #1, comment 10).

This OH exposure estimation improves Sect. 3.5 significantly, and as a result there is also better agreement between the TSAR and the PAM than in the first version of the manuscript. The figures 8, 9 and 10 were replaced with new ones because of the change in the OH exposure values (Figs. 10, 11 and 12 in the new manuscript).

9) Page 12, line 9-15: The discussion of the different toluene SOA yields among the Kang et al., Ng et al., and Hilderbrandt et al., is very brief and over-simplified. There are so many factors affecting the different studies that could potentially contribute to the reported SOA yields and differences cannot be explained only by the presence or absence of seed particles.

The aim of the toluene experiments were to compare the TSAR results to the PAM results at similar conditions. Thus, the comparison to other experiments (at different conditions) is now removed.

10) Page 12, line 18: The Aiken et al., (2008) analysis method for HR-AMS data has been updated by Canagaratna et al., (2015), with the new method having a direct effect on the reported O:C values. The authors should either justify the reason why they opted to use the Aiken calibration or update the results using the Canagaratna method.

At the time of the data treatment, the possibility to use Canagaratna method was not available in the software. The O:C values are now calculated using the Canagaratna method and the new values are applied to Figs. 11 and 12 (even though the difference is minimal). The text was changed as follows: "Elemental ratios are calculated using the method developed by Aiken et al. (2008) and improved by Canagaratna et al. (2015)."

Editorial comments:

Page 4, line 11: section should be 2.2 not 2.1 (same correction should be applied to all subsequent subsections in this part of the manuscript).

The section numbering is now corrected.

Page 10, line 14-16: the temperature and relative humidity should be reported as average with an associated standard deviation instead of the current mixing up of average with range.

References:

Peng et al., (2016), Non-OH chemistry in oxidation flow reactors for the study of atmospheric chemistry systematically examined by modeling. *Atmos. Chem. Phys.*, 16(7), 4283-4305.  
doi:10.5194/acp-16-4283-2016

The average values and associated standard deviation are now reported as suggested.

## References:

- Aiken, A. C., DeCarlo, P. F., Kroll, J. H., Worsnop, D. R., Huffman, J. A., Docherty, K. S., Ulbrich, I. M., Mohr, C., Kimmel, J. R., Sueper, D., Sun, Y., Zhang, Q., Trimborn, A., Northway, M., Ziemann, P. J., Canagaratna, M. R., Onasch, T. B., Alfarra, M. R., Prevot, A. S. H., Dommen, J., Duplissy, J., Metzger, A., Baltensperger, U. and Jimenez, J. L.: O/C and OM/OC Ratios of Primary, Secondary, and Ambient Organic Aerosols with High-Resolution Time-of-Flight Aerosol Mass Spectrometry, *Environ. Sci. Technol.*, 42(12), 4478–4485, doi:10.1021/es703009q, 2008.
- Gentner, D. R., Isaacman, G., Worton, D. R., Chan, A. W. H., Dallmann, T. R., Davis, L., Liu, S., Day, D. A., Russell, L. M., Wilson, K. R., Weber, R., Guha, A. and Harley, R. A.: Elucidating secondary organic aerosol from diesel and gasoline vehicles through detailed characterization of organic carbon emissions, , doi:10.1073/pnas.1212272109/- /DCSupplemental.www.pnas.org/cgi/doi/10.1073/pnas.1212272109, 2012.
- Gordon, T. D., Presto, A. A., May, A. A., Nguyen, N. T., Lipsky, E. M., Donahue, N. M., Gutierrez, A., Zhang, M., Maddox, C., Rieger, P., Chattopadhyay, S., Maldonado, H., Maricq, M. M. and Robinson, A. L.: Secondary organic aerosol formation exceeds primary particulate matter emissions for light-duty gasoline vehicles, *Atmos. Chem. Phys.*, 14(9), 4661–4678, doi:10.5194/acp-14-4661-2014, 2014.
- Huang, Y., Coggon, M. M., Zhao, R., Lignell, H., Bauer, M. U., Flagan, R. C. and Seinfeld, J. H.: The Caltech Photooxidation Flow Tube Reactor - I: Design and Fluid Dynamics, *Atmos. Meas. Tech. Discuss.*, (September), 1–36, doi:10.5194/amt-2016-282, 2016.
- Karjalainen, P., Timonen, H., Saukko, E., Kuuluvainen, H., Saarikoski, S., Aakko-Saksa, P., Murtonen, T., Bloss, M., Dal Maso, M., Simonen, P., Ahlberg, E., Svenningsson, B., Brune, W. H., Hillamo, R., Keskinen, J. and Rönkkö, T.: Time-resolved characterization of primary particle emissions and secondary particle formation from a modern gasoline passenger car, *Atmos. Chem. Phys.*, 16(13), 8559–8570, doi:10.5194/acp-16-8559-2016, 2016.
- Keller, A. and Burtscher, H.: A continuous photo-oxidation flow reactor for a defined measurement of the SOA formation potential of wood burning emissions, *J. Aerosol Sci.*, 49, 9–20, doi:10.1016/j.jaerosci.2012.02.007, 2012.
- Li, R., Palm, B. B., Ortega, A. M., Hlywiak, J., Hu, W., Peng, Z., Day, D. A., Knote, C., Brune, W. H., de Gouw, J. A. and Jimenez, J. L.: Modeling the Radical Chemistry in an Oxidation Flow Reactor: Radical Formation and Recycling, Sensitivities, and the OH Exposure Estimation Equation, *J. Phys. Chem. A*, 119(19), 4418–4432, doi:10.1021/jp509534k, 2015.
- Nordin, E. Z., Eriksson, a. C., Roldin, P., Nilsson, P. T., Carlsson, J. E., Kajos, M. K., Hellén, H., Wittbom, C., Rissler, J., Löndahl, J., Swietlicki, E., Svenningsson, B., Bohgard, M., Kulmala, M., Hallquist, M. and Pagels, J. H.: Secondary organic aerosol formation from idling gasoline passenger vehicle emissions investigated in a smog chamber, *Atmos. Chem. Phys.*, 13(12), 6101–6116, doi:10.5194/acp-13-6101-2013, 2013.
- Peng, Z., Day, D. A., Stark, H., Li, R., Lee-Taylor, J., Palm, B. B., Brune, W. H. and Jimenez, J. L.: HOx radical chemistry in oxidation flow reactors with low-pressure mercury lamps systematically examined by modeling, *Atmos. Meas. Tech.*, 8(11), 4863–4890, doi:10.5194/amt-8-4863-2015, 2015.
- Peng, Z., Day, D. A., Ortega, A. M., Palm, B. B., Hu, W., Stark, H., Li, R., Tsigaridis, K., Brune, W. H. and Jimenez, J. L.: Non-OH chemistry in oxidation flow reactors for the study of atmospheric chemistry systematically examined by modeling, *Atmos. Chem. Phys.*, 16(7), 4283–4305, doi:10.5194/acp-16-4283-2016, 2016.
- Platt, S. M., El Haddad, I., Zardini, A. A., Clairotte, M., Astorga, C., Wolf, R., Slowik, J. G., Temime-Roussel, B., Marchand, N., Ježek, I., Drinovec, L., Močnik, G., Möhler, O., Richter, R., Barmet, P., Bianchi, F., Baltensperger, U. and Prévôt, A. S. H.: Secondary organic aerosol formation from gasoline vehicle emissions in a new mobile environmental reaction chamber, *Atmos.*

- Chem. Phys., 13(18), 9141–9158, doi:10.5194/acp-13-9141-2013, 2013.
- Timonen, H., Karjalainen, P., Saukko, E., Saarikoski, S., Aakko-Saksa, P., Simonen, P., Murtonen, T., Dal Maso, M., Kuuluvainen, H., Ahlberg, E., Svenningsson, B., Pagels, J., Brune, W. H., Keskinen, J., Worsnop, D. R., Hillamo, R. and Rönkkö, T.: Influence of fuel ethanol content on primary emissions and secondary aerosol formation potential for a modern flex-fuel gasoline vehicle, *Atmos. Chem. Phys. Discuss.*, (September), 1–28, doi:10.5194/acp-2016-579, 2016.
- Tkacik, D. S., Lambe, A. T., Jathar, S., Li, X., Presto, A. A., Zhao, Y., Blake, D., Meinardi, S., Jayne, J. T., Croteau, P. L. and Robinson, A. L.: Secondary organic aerosol formation from in-use motor vehicle emissions using a potential aerosol mass reactor., *Environ. Sci. Technol.*, 48(19), 11235–11242, doi:10.1021/es502239v, 2014.

# A New Oxidation Flow Reactor for Measuring Secondary Aerosol Formation of Rapidly Changing Emission Sources

Pauli Simonen<sup>1</sup>, Erkkka Saukko<sup>1</sup>, Panu Karjalainen<sup>1</sup>, Hilkkka Timonen<sup>2</sup>, Matthew Bloss<sup>2</sup>, Päivi Aakko-Saksa<sup>3</sup>, Topi Rönkkö<sup>1</sup>, Jorma Keskinen<sup>1</sup>, and Miikka Dal Maso<sup>1</sup>

5 <sup>1</sup>Aerosol Physics Laboratory, Department of Physics, Tampere University of Technology, P.O. Box 692, FI-33101 Tampere, Finland

<sup>2</sup>Finnish Meteorological Institute, Atmospheric Composition Research, P.O. Box 503, FI-00101 Helsinki, Finland

<sup>3</sup>VTT Technical Research Centre of Finland Ltd., P.O. Box 1000, FI-02044 Espoo, Finland

*Correspondence to:* pauli.simonen@tut.fi

## 10 Abstract

Oxidation flow reactors or environmental chambers can be used to estimate secondary aerosol formation potential of different emission sources. Emissions from anthropogenic sources, such as vehicles, often vary on short timescales. For example, to identify the vehicle driving conditions that lead to high potential secondary aerosol emissions, rapid oxidation of exhaust is needed. However, the residence times in environmental chambers and in most oxidation flow reactors are too long to study these transient effects (~100 s in flow reactors and several hours in environmental chambers). Here, we present a new oxidation flow reactor, TSAR (TUT Secondary Aerosol Reactor), which has a short residence time (~40 s) and near-laminar flow conditions. These improvements are achieved by reducing the reactor radius and volume. This allows studying e.g. the effect of vehicle driving conditions on secondary aerosol formation potential of the exhaust. We show that the flow pattern in TSAR is nearly laminar and particle losses are negligible. The secondary organic aerosol (SOA) produced in TSAR has a similar mass spectrum as the SOA produced in the state-of-the-art reactor, PAM (Potential Aerosol Mass). Both reactors produce the same amount of mass, but the TSAR has a higher time-resolution. We also show that the TSAR is capable of measuring secondary aerosol formation potential of a vehicle during a transient driving cycle, and that the fast response of the TSAR reveals how different driving conditions affect the amount of formed secondary aerosol. Thus, the TSAR can be used to study rapidly changing emission sources, especially the vehicular emissions during transient driving.

25

30

35

## 1 Introduction

Aerosol particles in the atmosphere affect climate, health and visibility. To reduce these impacts, the sources of aerosol particles have to be resolved. One large but uncertain source of atmospheric aerosol particles is secondary organic aerosol (SOA) formation, which takes place in the atmosphere when particle mass forms as a result of atmospheric oxidation of organic precursor gases. Because the emission of precursor gases and the formation of secondary aerosol mass occur separately, the estimation of SOA sources and their magnitudes is difficult.

The total amount of atmospheric SOA is typically estimated using laboratory data of SOA yields for known precursors combined with their emission factors and emission profiles. (Kanakidou et al., 2005) However, the uncertainty of this method is high. For example, Kanakidou et al. (2005) estimate that approximately 10 % of global SOA is of anthropogenic origin, but measurements by Volkamer et al. (2006) show that the proportion can be as high as 33 %. Thus, more accurate estimations are needed to identify the most important SOA sources in order to identify the most efficient methods to decrease the human impact on aerosol loading in the atmosphere.

An alternative and more direct method to characterize SOA sources was introduced by Kang et al. (2007). Instead of measuring precursor gases and estimating the amount of potential SOA based on their yields, the SOA formation potential of a single emission source can be measured by oxidizing the emitted sample and measuring the secondary aerosol mass produced. This method reduces the uncertainty of the SOA emission magnitude, since unknown precursors as well as those whose measurement is difficult are taken into account.

Using this in situ method, emission oxidation and SOA formation process can be characterized using large environmental chambers, such as the one Platt et al. (2013) used when they measured the SOA potential of a gasoline vehicle. Another alternative is to use an oxidation flow reactor, in which the sample is oxidized in a similar manner but with higher oxidant concentrations than in large environmental chambers. Such a setup was first introduced by Kang et al. (2007), who also introduced their own oxidation flow reactor, the potential aerosol mass (PAM) chamber, hereafter referred to as PAM. The setup has been used e.g. to estimate the SOA formation potential of in-use vehicle emissions by sampling air from a highway tunnel (Tkacik et al., 2014), to measure the SOA formation from urban ambient air (Ortega et al., 2016) and to measure the SOA formation from ambient pine forest air (Palm et al., 2016). All these applications show the value of direct measurement of SOA potential, since the model results either over- or underestimated the SOA formation.

The use of an oxidation flow reactor instead of a large environmental chamber provides multiple advantages: short residence time, higher degree of oxidation and portability (Bruns et al., 2015). The short residence time allows high time-resolution measurements of constantly changing situations, so for example the effect of different test parameters on SOA formation can be studied in a shorter time than with environmental chambers. It is also possible to measure SOA formation of a changing emission source in real-time because of the short residence time. For example, ~~Karjalainen et al. (2015)~~ (Karjalainen et al., 2016) measured time-resolved SOA formation potential of a gasoline vehicle during a transient driving cycle using a PAM reactor. They observed that the secondary aerosol formation potential is highly dependent on the driving conditions. However, the PAM reactor is not ideal for rapidly changing emission sources such as vehicular emissions, since the residence time (~100 s) is still relatively long and the reactor outputs a distribution of different-aged aerosol (Lambe et al., 2011). This limitation is seen e.g. in (Karjalainen et al., 2016), where the cold start of a gasoline engine results in an exponentially decaying wide peak of SOA formed in PAM, whereas the concentration of total hydrocarbons measured from the exhaust shows much more transient behavior. Thus, the SOA formed in PAM cannot be linked directly to the emissions. To address this limitation, the residence time must be shortened. An ultimate example of a short-residence time flow reactor is the micro-smog chamber

(MSC) with residence time < 10 s (Keller and Burtscher, 2012). However, (Bruns et al., (2015) show that the composition and amount of the SOA produced in MSC usually differs from those of the SOA produced in PAM or in an environmental chamber, possibly because of insufficient time for condensation of oxidant products. Thus, a compromise between PAM and MSC is needed for studying rapidly changing emissions: shorter residence time than in PAM but still long enough to allow the condensation on aerosol phase.

In this work, we introduce and present a characterization of a new oxidation flow reactor, the *TUT Secondary Aerosol Reactor (TSAR)*. The TSAR is better suited to measuring the real-time secondary aerosol formation potential of rapidly changing emission sources than the state-of-the-art oxidation flow reactors due to its improved flow conditions and shorter residence time. In the following sections, we characterize the TSAR by describing its particle losses, oxidant exposure, residence time distribution, laboratory studies on sulfur acid yield as well as toluene SOA yield and properties, including a comparison between PAM and TSAR. In addition, we present measurements of the secondary aerosol formation of gasoline vehicle emissions during a transient driving cycle. We show that the fast response of TSAR gives valuable information on the effect of the driving condition on secondary aerosol formation potential.

Because of the high oxidant concentrations, high UV light intensity at non-tropospheric wavelengths and limited time for the condensation, atmospheric implications cannot be directly drawn from flow reactor measurements. However, there are no methods to measure the absolute secondary aerosol formation potential, because the environmental chambers also have their drawbacks (e.g. limited oxidant exposure and inability to measure time-resolved secondary aerosol potential) (Bruns et al., 2015). Despite these artifacts, there is a need for estimation of secondary aerosol formation from different emission sources. Thus, also the flow reactor results provide useful information, on condition that a proper error analysis is made. In this work, we address the flow-reactor related artefacts of TSAR by modeling the vapor losses caused by photolysis and the short residence time.

## 2 Experimental

### 2.1 Oxidation flow reactor

TSAR is an OFR-254 type oxidation flow reactor, according to terminology proposed by Li et al. (2015), which means that OH radicals are produced from the photolysis of the ozone at 254 nm UV radiation. Its layout is presented in Fig. 1 (see Fig. S3 for a photograph). The TSAR consists of a residence time chamber (1 in Fig 1), an oxidation reactor (3), an ozone generator, three mass flow controllers and an expansion tube (2) that connects the residence time chamber and oxidation reactor. The residence time chamber is a 50 cm x 5 cm ID stainless steel cylinder that ensures the mixing of the sample and makes the sample flow laminar before entering the oxidation reactor. The half cone angle of the expansion tube is 6 degrees. Two of the mass flow controllers are connected to a vacuum line and are used to control the flow rates inside the residence time chamber and the oxidation reactor. The excess flow from the oxidation reactor is hereafter called “secondary excess flow”. The third mass flow controller adjusts the air flow through the ozone generator. All the components except the residence time chamber and the expansion tube are located inside a single housing, which makes TSAR easy to transfer to different measuring environments.

The TSAR oxidation reactor is a 3.3 l (52 cm x 9 cm inner diameter) quartz glass cylinder surrounded by two constant power ozone free low pressure mercury lamps which emit 254 nm UV light. The lamps are placed outside the reactor to ensure laminar flow and to decrease the surface-to-volume ratio. The UV radiation generates excited oxygen atoms [O(1D)] from the photolysis of O<sub>3</sub>. These atoms react with water molecules, producing OH radicals. The O<sub>3</sub> needed for this reaction chain is

mixed with the sample prior to the residence time chamber. In some cases, the humidity of the sample is too low for sufficient OH generation and additional humidification is required; in these cases, humidified air is also mixed into the sample at this point. If the lamps emitted also 185 nm UV light, no external ozone generator would be needed and the TSAR would operate in OFR185 mode. However, we chose the OFR254 mode because of the poor transmission efficiency of the quartz glass for 185 nm light. In addition, the 185 nm light would generate ozone in the room air, which would require a special ventilation for the TSAR casing to avoid health issues.

The ozone is generated by an external ozone generator (either Model 600 or Model 1000, Jelight Company Inc.), which produces ozone from oxygen photolysis by 185 nm UV radiation. The ozone concentration can be adjusted by partially covering the UV lamp (Model 600) or by adjusting the flow rate through the generator.

The TSAR outlet is a 10 mm OD stainless steel probe, and its axial position can be adjusted, so that the oxidized sample can be measured from any distance from the inlet. From the probe, the sample is led to the measurement devices or to an ejector diluter, which allows the use of multiple instruments while maintaining a constant flow through the oxidation reactor.

## 2.21 Residence time distribution experiments

The flow conditions inside the TSAR oxidation reactor affect the dynamic transfer function  $E(t)$  of the reactor for non-reacting compounds. For this case, the measured temporal output concentration  $C_{out}(t)$  of the TSAR for a measured dynamic input concentration  $C_{in}(t)$  is the convolution of the measured input concentration and the transfer function (Fogler, 2006):

$$C_{out}(t) = E(t) * C_{in}(t) \quad (1)$$

The transfer function  $E(t)$  also is the unit impulse response of the reactor or the residence time distribution following an ideal Dirac delta input impulse. To test the response function, ten-second square pulses of CO<sub>2</sub> were injected into the TSAR mixed with pressurized air. To keep the shape of the CO<sub>2</sub> pulse as sharp as possible, the volumetric flow rate in the residence time chamber was kept at 50 slpm. In the oxidation reactor the flow rate was 5 slpm. CO<sub>2</sub> concentration was measured with a CO<sub>2</sub> analyzer (Sidor, Sick Maihak). As the same instrument is used for the measurement of both input and output concentrations, its response function is imbedded both in  $C_{in}(t)$  and  $C_{out}(t)$ .

First, three separate CO<sub>2</sub> pulses were measured with sampling at the end of the residence time chamber. The outlet probe was then adjusted to sample at the end of the oxidation reactor and three separate pulses were again measured. The residence time distributions were determined for different situations: UV lamps and the secondary excess flow were either on or off.

## 2.32 Particle loss quantification

Particle losses in the oxidation reactor were measured using dioctyl sebacate (DOS) particles with mobility diameter from 20 to 100 nm and silver particles from 5 to 30 nm. The DOS particles were generated by atomizing DOS-isopropanol solution. The silver particles were generated with an evaporation-condensation technique (Harra et al., 2012). In these experiments, the volumetric flow in both the residence time chamber and oxidation reactor was 5 slpm.

A narrow monodisperse particle size distribution, size-selected using a differential mobility analyzer (nano-DMA, TSI Inc. Model 3085), was injected into the TSAR. The particle number concentration was measured with an ultrafine condensation particle counter (UCPC, TSI Inc. Model 3025) before and after the oxidation reactor using the adjustable outlet probe. This procedure was repeated two or three times for each particle size.

## 2.4 OH exposure experiments

The length of the duration of atmospheric oxidation that the oxidation flow reactor simulates is determined by exposure of the sample to OH radicals. OH exposure ( $OH_{exp}$ ) is defined as  $[OH] \times t$ , where  $[OH]$  is the mean OH radical concentration in the oxidation reactor and  $t$  is the mean residence time of sample in the reactor.  $OH_{exp}$  could be measured indirectly by monitoring the loss of  $SO_2$  in the reactor. (Lambe et al., 2011) Since the only significant loss of  $SO_2$  in the oxidation reactor is due to the reaction with OH radicals (and possible wall loss), the change in  $SO_2$  concentration is defined by the following differential equation:

$$\frac{d[SO_2]}{dt} = -k_{OH+SO_2}[OH][SO_2] - k_{wall}[SO_2], \quad (2)$$

10 where  $[SO_2]$  is the  $SO_2$  concentration, ~~and~~  $k_{OH+SO_2}$  is the reaction rate constant and  $k_{wall}$  is the first-order wall loss for  $SO_2$ . From this, we get the OH exposure

$$OH_{exp} = \frac{1}{k_{OH+SO_2}} \ln \frac{[SO_2]_0}{[SO_2]_f}, \quad (3)$$

where  $[SO_2]_0$  and  $[SO_2]_f$  are the  $SO_2$  concentrations of the sample before and after oxidation, respectively. Because both  $[SO_2]_0$  and  $[SO_2]_f$  are measured after the TSAR, the first without UV lights and the latter with UV lights, the wall loss term  
15 cancels out from the equation.

Because the OH radicals are produced in a reaction between water molecules and  $O(^1D)$  atoms produced by ozone photolysis, both humidity and ozone concentration affect the amount of OH radicals (Seinfeld and Pandis, 1998).  $OH_{exp}$  was measured using three different relative humidities (15 %, 30 % and 45 %) and several different ozone concentrations (0.6 ppm–49 ppm).  
20 ~~Pressurized air,  $SO_2$ , Humidified air, and ozone~~ and  $SO_2$  diluted with pressurized air were injected into the TSAR to determine the OH exposure. First, humidity, ozone concentration and  $[SO_2]_0$  were measured after the TSAR. Then the UV lamps were turned on, and the concentration rapidly decreased and stabilized to the value of  $[SO_2]_f$ .  $SO_2$  concentration was measured with AF22M analyzer (Environnement S.A) and ozone with model 205 analyzer (2B Technologies).

25 Based on the  $OH_{exp}$  measurements, it is possible to deduce the UV actinic flux in the TSAR by reproducing the results in a photochemical model and using the photon flux as a fitting parameter. We used the model available in PAM users manual (PAM chem v8 by William Brune, <https://sites.google.com/site/pamusersmanual/7-pam-photochemistry-model/a-introduction>), which is similar to the model described by (Li et al., (2015). In this model, the differential equations describing the chemical reactions are solved using Euler's method (instead of Runge-Kutta method used in the model by (Li et al., (2015)).

## 30 2.5 ~~Estimating vapor losses and photolysis~~ Sulfuric acid yield experiments

In an ideal oxidation flow reactor, all the condensable vapors condense onto particle phase and will be measured as potential secondary aerosol mass. However, there are also other pathways than condensation for the vapors in the flow reactor, and some of them are non-tropospheric. First, the intensity of the UV radiation is higher and the wavelength is smaller than those of the UV radiation in the troposphere. This can cause unrealistic photolysis of the precursor vapors and the secondary aerosol formed  
35 (Peng et al., 2016). Second, the residence time in the flow reactor is small, and thus the condensable vapors may exit the reactor before condensing onto particle phase. Third, because of high oxidant concentrations, the timescale of condensation can be much higher than the timescale of oxidation, leading to fragmentation of oxidized vapor molecules before they have condensed. This is of concern especially in the TSAR, where the short residence time requires higher oxidant concentrations than e.g. PAM chamber. Fourth, the surface-area-to-volume ratio is high in the flow reactor, and thus the vapor wall losses may be  
40 significant. (Palm et al., 2016)

### 2.5.1 Photolysis

(Peng et al., (2016) have studied the losses of precursor gases and SOA due to photolysis in flow reactors. In their study, they show that the photolysis rate of SOA in oxidation flow reactors is uncertain because of the lack of knowledge on quantum yields. In any case, the loss of SOA due to photolysis is much smaller in oxidation flow reactors than in the troposphere at equivalent OH exposure. However, the photolytic losses of precursor gases in oxidation flow reactors can be higher than in the troposphere.

The photolytic loss is significant if the photolysis rate is high relative to reaction rate with OH radical. We define relative photolytic loss as

$$relative\ photolytic\ loss = \frac{photolysis\ rate\ at\ 254\ nm}{photolysis\ rate\ at\ 254\ nm + reaction\ rate\ with\ OH} \quad (4)$$

A relative photolytic loss of zero means that all the loss of the precursor gas is due to reaction with OH, and relative photolytic loss of unity means that the photolysis is the only pathway of loss for the precursor gas. As Peng et al. (2016) show, the relative photolytic loss depends on the ratio of photon exposure to OH exposure ( $F_{254_{exp}}/OH_{exp}$ ), the reaction rate constant between the precursor molecule and OH radical, the absorption cross section of the molecule and the quantum yield of the photolysis reaction. The OH exposure in the TSAR depends on water vapor concentration ( $[H_2O]$ ), ozone concentration and external OH reactivity of the sample ( $OHR_{ext} = [X] \cdot k_{OH+X}$ , where  $[X]$  is the precursor gas concentration and  $k_{OH+X}$  is the reaction rate constant between this gas molecule and OH radical). The photon flux in TSAR is constant.

According to the modeling results by Peng et al. (2016), the relative photolytic loss of studied precursor gases is less than 60 % in most cases in OFR254, even at “riskier” conditions ( $[H_2O] < 0.1\%$  or  $OHR_{ext} > 200\ s^{-1}$ ). For most of the studied precursor gases, the relative photolytic loss is less than 20 % in most cases. In all the studied “safer” conditions ( $[H_2O] > 0.5\%$  and  $OHR_{ext} < 50\ s^{-1}$ ), the relative photolytic loss is less than 30 % for all the precursor gases. However, these are only the upper limits for the relative photolytic losses because of the assumption of a unity quantum yield. The relative photolytic losses in TSAR are discussed in Sect. 3.4.1.

### 2.5.2 Vapor losses

We study the fate of condensable vapors (other than photolysis) in TSAR using a similar approach as (Palm et al., (2016). We start with a low-volatile organic compound (LVOC, saturation vapor concentration  $\sim 0$ ) which can condense on particle phase, condense on the reactor walls, form new particles via nucleation, react with OH radical or exit the reactor before condensing.

Thus, the concentration of the LVOC is described with the following differential equation

$$\frac{dC_0}{dt} = -4\pi \cdot D \cdot CS \cdot C_0 - k_w \cdot C_0 - k_{OH} \cdot C_0 \cdot [OH] - n \cdot J(C_0) \quad (5)$$

where  $C_0$  is the concentration of the initial LVOC,  $D$  is the diffusion coefficient of the LVOC,  $CS$  is the condensational sink,  $k_w$  is first-order rate coefficient for wall-loss,  $k_{OH}$  is the reaction rate constant between OH radicals and the LVOC,  $[OH]$  is the mean concentration of OH radicals in the reactor,  $n$  is the number of molecules in a nucleated particle and  $J$  is the nucleation rate, which depends on the vapor concentration. We assume that the reaction with OH radical produces another LVOC ( $C_1$ ) which has the same loss terms as  $C_0$ . Thus,

$$\frac{dC_1}{dt} = k_{OH} \cdot C_0 \cdot [OH] - 4\pi \cdot D \cdot CS \cdot C_1 - k_w \cdot C_1 - k_{OH} \cdot C_1 \cdot [OH] - n \cdot J(C_1) \quad (6)$$

and more generally,

$$\frac{dC_n}{dt} = k_{OH} \cdot C_{n-1} \cdot [OH] - 4\pi \cdot D \cdot CS \cdot C_n - k_w \cdot C_n - k_{OH} \cdot C_n \cdot [OH] - n \cdot J(C_n) \quad (7)$$

assuming that  $k_{OH}$ ,  $D$ ,  $CS$ ,  $k_w$ ,  $n$  and  $J$  are equal for all oxidation products.

At some point, the reaction between LVOC and OH radical leads to fragmentation and produces high-volatility compounds which cannot condense onto particle phase. Palm et al. (2016) assumed that the fifth oxidation reaction produces fragmented compounds. In addition, the heterogeneous OH reaction on the particle surface may result in fragmentation (Kroll et al., 2009).

5 Thus, assuming that the molecule fragments to two parts, we get

$$\frac{dC_5}{dt} = 2 \cdot k_{OH} \cdot C_4 \cdot [OH] + 2 \cdot R_{heterogeneous} \quad (8)$$

where  $C_5$  is the mass concentration of fragmented, high-volatility compounds and  $R_{heterogeneous}$  is the rate of heterogeneous fragmentation. Based on these equations, the molecule flux to the aerosol phase is

$$\frac{dC_{aer}}{dt} = 4\pi \cdot D \cdot CS \cdot (C_0 + C_1 + C_2 + C_3 + C_4) - R_{heterogeneous} \quad (9)$$

10 and the mass flux to the reactor walls is

$$\frac{dC_w}{dt} = k_w \cdot (C_0 + C_1 + C_2 + C_3 + C_4) \quad (10)$$

The fate of LVOC is obtained by solving the differential equations using MATLAB (Release 2016a, The MathWorks, Inc., United States) ode45 numerical solver. The fraction of LVOC lost to walls is then

$$15 F_{wall} = \frac{C_w(\tau_{res})}{C_0(0)} \quad (11)$$

where  $\tau_{res}$  is the residence time of the reactor and  $C_0(0)$  is the initial LVOC concentration. Similarly, the fraction of LVOC condensed onto aerosol is

$$F_{aer} = \frac{C_{aer}(\tau_{res})}{C_0(0)} \quad (12)$$

the fragmented fraction is

$$20 F_{frag} = \frac{1}{2} \frac{C_5(\tau_{res})}{C_0(0)} \quad (13)$$

and finally, the fraction of LVOCs that exit the reactor before condensing is

$$F_{exit} = \frac{C_0(\tau_{res}) + C_1(\tau_{res}) + C_2(\tau_{res}) + C_3(\tau_{res}) + C_4(\tau_{res})}{C_0(0)} \quad (14)$$

Looking at Eqs. (5-8), the OH radical concentration affects the relative amount of LVOC that is fragmented. The shorter the residence time, the higher the [OH] must be to attain a certain OH exposure. Thus, shortening the residence time results in increase in fragmented LVOC. However, the fragmented fraction depends on the timescales of the other loss terms, namely condensation on reactor walls and on aerosol that in turn depends on the condensational sink. Using this approach, the dependence of LVOC fate on residence time and condensational sink are studied in Sect 3.4.2.

30 We tested the model validity by oxidizing SO<sub>2</sub> in the TSAR. SO<sub>2</sub> oxidation is a simple example of secondary aerosol formation. SO<sub>2</sub> reacts with OH radicals to produce sulfuric acid (H<sub>2</sub>SO<sub>4</sub>) vapor which rapidly enters the particle phase by nucleation and condensation (Sihto et al., 2006). The mass formed by oxidation of SO<sub>2</sub> can be theoretically calculated from the SO<sub>2</sub> loss, and thus comparing the measured mass formation to the theoretical prediction can be used to estimate the capability of TSAR to simulate full atmospheric oxidation. Should the measured mass be substantially smaller than the theoretical, we would assume  
 35 that there are significant losses of sulfuric acid vapor inside TSAR. ~~This would then also mean that the losses for organic low-volatile and semi-volatile vapors were also high.~~ The observed losses can then be compared to the losses predicted by Eqs. (11-14).

The sulfuric acid yield was measured by injecting ~~pressurized air, SO<sub>2</sub>, humidified air and~~ ozone and SO<sub>2</sub> diluted with  
 40 ~~pressurized air~~ into the TSAR. The relative humidity and SO<sub>2</sub> was measured straight after TSAR, whereas ozone concentration

and the particle size distribution were measured after an ejector dilutor (Dekati Ltd.). The dilution ratio was determined by measuring the sample flow rate and the dilution air flow rate. The particle size distribution was measured with a nano-SMPS (scanning mobility particle sizer: a nano-DMA (TSI Inc. model 3085) combined with a UCPC (TSI Inc. model 3025)).

5 In addition to sulfuric acid, the measured particles also contain water. The sulfuric acid mass was calculated from Eq. (415) (Lambe et al., 2011).

$$m_{H_2SO_4} = \chi_{H_2SO_4} \times V \times \rho, \quad (415)$$

where  $\chi_{H_2SO_4}$  is the mass fraction of sulfuric acid in the particle phase,  $V$  is the volume calculated from nano-SMPS particle size distribution and  $\rho$  is the density of the particle phase. Both the mass fraction and the density were calculated as a function of relative humidity based on Seinfeld and Pandis (1998). In the calculations, relative humidity after the dilution is used, assuming fast equilibration of the sulfuric acid particles.

The theoretical (maximum) sulfuric acid mass was calculated by multiplying the loss of  $SO_2$  by the molar mass of a sulfuric acid molecule. Thus, the loss of 1 ppb of  $SO_2$  produces  $4.03 \mu\text{g m}^{-3}$  of sulfuric acid aerosol, assuming also that all the sulfuric acid condenses into the particle phase.

## 2.6 Organic precursor experiments

A key application of TSAR is to estimate the amount of secondary aerosol mass formed from engine exhaust emissions, which in turn contains a complex mixture of organic and inorganic gases. Therefore, the  $SO_2$  oxidation experiment alone is not a representative example of engine exhaust oxidation, because the oxidation pathways of organic compounds are far more complex. The ability of TSAR to form SOA was verified by measuring the toluene SOA obtained by TSAR and the PAM simultaneously. Previous studies have shown that the amount and properties of the SOA produced in the PAM are similar to those of the SOA formed in smog chambers, ~~which represent atmospheric oxidation~~ (Bruns et al., 2015; Lambe et al., 2015).

The organic precursor gas in this experiment was toluene, because it is present in engine exhaust gas (Peng et al., 2012; Wang et al., 2013). In addition, toluene is globally one of the most emitted anthropogenic SOA precursors (Kanakidou et al., 2005). Gas-phase toluene was produced using a permeation oven with a toluene permeation tube (KIN-TEK Laboratories Inc.), and its output rate ( $\dot{M}_{toluene}$ ) was measured by weighing the change in its mass. The concentration of toluene in the reactors is

$$C_{toluene} = \frac{\dot{M}_{toluene}}{Q_{tot}}, \quad (516)$$

where  $Q_{tot}$  is the total sample flow through the reactors (10 slpm).

The gas-phase toluene was mixed with ozone and humidified air before it was fed to the TSAR residence time chamber. After the residence time chamber, 5 slpm of the sample was introduced into the TSAR oxidation reactor and 5 slpm to the PAM. A 4-way valve was installed after the reactors, so that the instruments were sampling from one reactor while the sample from the other reactor was drawn to the vacuum line through a mass flow controller.

The PAM was used in OFR185 mode (Li et al., 2015) and thus the external ozone generator was switched off when the instruments were sampling from the PAM. The PAM was operated in OFR185 mode instead of OFR254 mode because the OFR185 mode is used in previous engine exhaust studies (Karjalainen et al., 2016; Timonen et al., 2016; Tkacik et al., 2014). Similar results from the two reactors would then indicate that the TSAR operating in OFR254 mode can be used in similar applications as the PAM in OFR185 mode. The  $OH_{exp}$  of the reactors was varied by varying the light intensity in the PAM and the amount of injected ozone in the TSAR. The PAM  $OH_{exp}$  as a function of output ozone concentration was measured

off-line in a similar way as for TSAR (Sect. 2.4) at 28 % relative humidity. The PAM reactor  $OH_{exp}$  as a function of output ozone concentration is shown in Fig. S1.

The particle size distribution downstream of TSAR and PAM was measured with an SMPS (Model 3081 DMA and Model 3775 CPC, TSI Inc.) and in some experiments also with an engine exhaust particle sizer (EEPS, TSI Inc.) (Johnson et al., 2004). The EEPS sample had to be diluted with a mass flow controller to keep the total flow rate through chambers at 5 slpm. Aerosol chemical composition and size distribution were measured with an SP-AMS (Soot-particle aerosol mass spectrometer, Onasch et al., 2012). In addition, the ozone concentration (Model 205, 2B Technologies) and relative humidity (Hygroclip SC05, Rotronic AG) were measured.

10

Two different toluene experiments were run: steady state and pulse experiments. In the steady state experiments, a constant concentration of toluene was continuously injected into the reactors. Based on these experiments, the toluene SOA yield was determined for both reactors.

15 The pulse experiments were performed to study the reactors' behavior during rapid changes of toluene concentration. In these experiments, toluene was injected through a 3-way solenoid valve to either the reactors, or to the excess line. Three different pulse experiments were performed: a single 10 second pulse, and two different cycles with several pulses (cycle 1 and cycle 2). In cycle 1, three toluene pulses were injected with intervals of 10 and 15 seconds, whereas cycle 2 had intervals of 40 and 50 seconds. The cycles are described in detail in Table 1.

20

In both cycles, the total toluene injection time was 25 seconds and therefore the total amount of injected toluene was equal. The EEPS was used to measure the particle number distribution of produced SOA at a time resolution of one second. For the pulse experiments, the flow rate through each reactor was 5 slpm. Since the PAM is approximately ~~twice-four times as big as bigger than~~ TSAR in volume, also a 10 slpm flow rate was used for the PAM to compare the reactors at more similar ~~theoretical residence mean plug-flow residence~~ times. In this case, the TSAR was bypassed to keep the total flow at 10 slpm.

25

The SOA yield ( $Y$ ) is defined as the produced organic aerosol mass ( $\Delta M$ ) per reacted precursor mass ( $\Delta HC$ ) (Odum et al., 1996):

$$Y = \frac{\Delta M}{\Delta HC} \quad (617)$$

30 The amount of reacted toluene mass depends on the  $OH_{exp}$ ; the change in toluene concentration is defined by a similar differential equation as the change in  $SO_2$  concentration (Eq. (2)). Thus, the amount of reacted toluene is

$$\Delta[toluene] = [toluene]_0(1 - \exp(-k_{OH+toluene} \times OH_{exp})), \quad (187)$$

where  $[toluene]_0$  is the initial toluene concentration and  $k_{OH+toluene}$  is the reaction rate constant between toluene and OH radicals. A rate constant of  $6.18 \times 10^{-12} \text{ cm}^3 \text{ s}^{-1}$  was used based on the parameters presented by Atkinson (1985).

## 35 2.7 Vehicle exhaust experiments

The ability of TSAR to produce secondary aerosol mass from engine exhaust emissions was evaluated by sampling the exhaust of a Euro 5 GDI light-duty vehicle during a transient driving cycle (New European Driving Cycle, NEDC) run on a chassis dynamometer. The official cycle begins with a cold engine start, but in this study the NEDC was run with a warm engine and this is hereafter called a *warm NEDC*. Prior to the warm NEDC, the vehicle was run at  $80 \text{ km h}^{-1}$  for at least 3 minutes, and 40 the cycle began with an idling engine.

The sampling setup of vehicle exhaust experiments is shown in Fig. S2. The engine exhaust was sampled from the tailpipe using a porous-tube diluter (PTD) followed by a short cylindrical residence time chamber with residence time of 2.9 s. Dilution air temperature was 30 °C and dilution ratio approximately 12. This dilution setup has been shown to mimic the atmospheric cooling and dilution processes of primary aerosol reasonably well (Keskinen and Rönkkö, 2010; Rönkkö et al., 2006). The exact dilution ratio of the PTD was determined by CO<sub>2</sub> measurements from the tailpipe and after the PTD. After the residence time chamber, 3 slpm of humidified air and 3 slpm of ozone were mixed with the sample. At this stage, the dilution ratio was 2.5. Thus, the total dilution ratio before TSAR was approximately 30. The sample from TSAR was drawn through an active carbon ozone scrubber to an ejector diluter (Dekati Ltd.) at 5 slpm flow rate. The total dilution ratio between the tailpipe and instruments was determined by CO<sub>2</sub> measurements which were performed during 80 km h<sup>-1</sup> steady state driving, when the CO<sub>2</sub> concentration in the tailpipe was stable.

The particle size distributions were measured with EEPS, Electrical low-pressure impactor (ELPI+, Dekati Ltd.) and High-resolution low-pressure cascade impactor (HRLPI)(Arffman et al., 2014). CO<sub>2</sub> concentration after tailpipe was measured with Sick Maihak CO<sub>2</sub> analyzer, using a sample drier prior to the analyzer. Relative humidity and sample temperature were measured after TSAR using an RH sensor (Hygroclip SC05, Rotronic AG).

The amount of secondary aerosol mass produced in TSAR was determined by subtracting the primary mass from the mass measured when using the TSAR. Primary aerosol was measured with the same setup by operating the TSAR with UV lamps and the ozone generator turned off. The primary emission was measured during two warm NEDCs.

20

In this setup, the sample flow from the tailpipe is constant regardless of the exhaust mass flow. To determine the emission factors, the measured concentrations are multiplied with the corresponding exhaust mass flow.

### 3 Results and discussion

#### 3.1 Residence time distribution

The evolution of a CO<sub>2</sub> pulse in the TSAR is shown in Fig. 2. A narrow pulse enters the oxidation reactor and exits the reactor as a broader pulse. The theoretical transfer function of the oxidation reactor is calculated based on the residence time distribution of ideal laminar flow:

$$E(t) = \begin{cases} 0 & , t < \frac{\tau}{2} \\ \frac{\tau^2}{2t^3} & , t \geq \frac{\tau}{2} \end{cases} \quad (819)$$

where the constant  $\tau$  is defined as

$$\tau = \frac{\pi R^2 L}{Q}, \quad (920)$$

where  $R$  is the inner radius of the reactor,  $L$  is the length of the reactor and  $Q$  is the flow rate. (Fogler, 2006)

Figure 2 shows both the measured pulse after the reactor and the modeled pulse calculated according to Eq. (1) using the theoretical transfer function and the measured input concentration.

35

As seen in Fig. 2, the measured pulse is somewhat broader than the modeled one. There are some possible reasons for this discrepancy: first, the flow inside the reactor is probably not totally laminar because of the expansion in diameter between the residence time chamber and the oxidation reactor, and because of the abrupt diameter change at the end of the reactor; second, the pulse becomes broader in the sampling lines, which is not taken into account here.

In Fig. 2, UV lamps are turned off and the secondary excess flow is on. Because both of these affect the flow, the residence time distribution was measured for different combinations of these parameters, and the results are shown in Fig. 3. In all cases, the total flow rate through the oxidation reactor was 5 slpm. Because the incoming pulse is not an ideal Dirac delta function, the residence time distribution cannot be calculated with Eq. (8). Instead, the residence time distribution is the measured concentration  $C_{out}(t)$  divided by the total area of the pulse (Fogler, 2006)

$$RTD(t) = \frac{C_{out}(t)}{\int_0^{\infty} C_{out}(t) dt} \quad (421)$$

Turning off the secondary excess flow broadens the distribution slightly, probably because there is more dead volume at the end of the reactor. Turning the UV lamps on has a similar effect. The UV lamps heat the reactor walls and cause convection inside the reactor. This effect could be reduced by circulating air through the TSAR housing, but on the other hand small heating of the reactor walls may decrease the vapor wall losses. Another method to reduce the convection is to place the reactor vertically.

The residence time distributions show that the flow in the TSAR oxidation reactor is near-laminar. Thus, the mean residence time of the sample in the reactor can be calculated with Eq. (422) (Fogler, 2006)

$$t_{mean} = \frac{\tau}{2} = \frac{\pi R^2 L}{2Q}, \quad (422)$$

which yields 37 seconds at 5 slpm flow rate. Turning off the secondary excess flow reduces the laminarity, but this is often necessary to keep the flow rate at 5 slpm since for example an ejector diluter alone draws approximately 5 slpm of sample. In any case, the residence time distribution is clearly narrower, and the mean residence time is shorter than those of the PAM (Lambe et al., 2011), allowing the measurements of rapidly changing emission sources.

### 3.2 Particle losses

The particle transmission efficiency as a function of particle mobility diameter is presented in Fig. 4, as well as the theoretical diffusive losses of particles in a tube with laminar flow (Brockmann, 2011). The markers indicate the particle material, and error bars denote the standard deviation between separate experiments.

Figure 4 shows that the measured transmission efficiency agrees well with the theoretical efficiency, as expected, and thus the losses are less than 10 % when the particle mobility diameter is larger than 5 nm. Therefore, the results in the next sections are not corrected with this efficiency curve because the particle losses are negligible.

According to Lambe et al. (2011), the transmission efficiency of particles is significantly lower in the PAM: less than 70 % for particles smaller than 100 nm. Since the flow in TSAR is near-laminar, it is not surprising that the measurements agree with the theory. In PAM, the residence time distribution is broad, allowing more time for the particles to diffuse onto walls (and possibly to coagulate or evaporate), resulting in a non-ideal transmission efficiency.

### 3.3 OH exposure

Figure 5 shows that the OH exposure in TSAR oxidation reactor is sensitive to ozone concentration at low concentrations, but levels off to a near-constant value when the concentration is higher than 25 ppm. The  $OH_{exp}$  also depends on the relative humidity. The maximum  $OH_{exp}$  at 30 % RH is approximately  $1.2 \times 10^{12}$  molec. s  $cm^{-3}$ , equivalent of 9 days of atmospheric OH exposure, whereas in the PAM, up to 17 days of equivalent exposure are reached (Lambe et al., 2015; See also Fig. S1). In the calculation of the equivalent atmospheric exposure, an average OH concentration of  $1.5 \times 10^6$  molec.  $cm^{-3}$  in the

atmosphere is assumed (Mao et al., 2009). TSAR OH exposure could be further increased by increasing the RH or by increasing the UV lamp wattage.

The measurement results could be reproduced in the photochemical model using the photon flux, first-order OH radical wall loss and first-order ozone wall loss as free parameters. The best fit values are  $1.92 \times 10^{15}$  photons  $\text{cm}^{-2} \text{s}^{-1}$  (254 nm photon flux),  $8.3 \text{ s}^{-1}$  (OH wall loss) and  $7.5 \times 10^{-4} \text{ s}^{-1}$  (ozone wall loss). Using these parameters, the model predicts the measurement results within  $\pm 20\%$  uncertainty when the relative humidity, temperature, initial ozone concentration and initial  $\text{SO}_2$  concentration are used as the input parameters (Fig. S4).

### **3.4 Sulfuric acid Vapor losses and photolysis in TSAR**

#### **3.4.1 Photolysis**

Based on the modeling results in Sect. 3.3, the flux of 254 nm photons in TSAR is  $1.92 \times 10^{15}$  photons  $\text{cm}^{-2} \text{s}^{-1}$  and does not depend on OH exposure, since OH exposure is adjusted by  $\text{O}_3$  and  $\text{H}_2\text{O}$  concentration. Assuming residence time of 37 seconds (Sect. 3.1), the ratio  $F_{254\text{exp}}/\text{OH}_{\text{exp}}$  is shown in Fig. 6a. When the  $\text{OH}_{\text{exp}} > 10^{11} \text{ molec. cm}^{-3} \text{ s}$  ( $\sim 0.8$  days equivalent atmospheric exposure), the ratio is less than  $10^6 \text{ cm s}^{-1}$ . According to Peng et al. (2016), the relative photolytic loss for most VOCs is below 20% at this ratio. The only exceptions are acetylacetone, E,E,2,4-hexadienedial, peroxyacetyl nitrate and species with multiple hydroxyls and carbonyls, whose relative photolytic loss is 30-60% when  $F_{254\text{exp}}/\text{OH}_{\text{exp}}$  is  $10^6$ . At higher  $\text{OH}_{\text{exp}}$ , the relative photolytic losses decrease. Thus, to avoid non-tropospheric photolysis of precursor gases, the OH exposure must be maintained high enough. However, we note that these relative photolytic losses are upper limits, since a unit quantum yield is assumed in the calculations.

As shown by (Peng et al., (2015)), the  $\text{OH}_{\text{exp}}$  in OFR254 depends on water vapor concentration,  $\text{OHR}_{\text{ext}}$ , photon flux and ozone concentration. Using the photochemical model described in Sect. 2.4, we evaluate the effect of  $\text{OHR}_{\text{ext}}$  on  $F_{254\text{exp}}/\text{OH}_{\text{exp}}$  while keeping the temperature, relative humidity and initial ozone concentration constants ( $20^\circ\text{C}$ , 30% and 45 ppm, respectively). According to the model results (Fig. 6b),  $F_{254\text{exp}}/\text{OH}_{\text{exp}} < 10^6 \text{ cm s}^{-1}$  as long as  $\text{OHR}_{\text{ext}} < 2500 \text{ s}^{-1}$ . On the other hand, the  $\text{OH}_{\text{exp}}$  decreases as a function of  $\text{OHR}_{\text{ext}}$ . A worst-case scenario regarding the  $\text{OHR}_{\text{ext}}$  in exhaust measurements is a cold engine start, where the  $\text{OHR}_{\text{ext}}$  can be as high as  $1000 - 3400 \text{ s}^{-1}$  (excluding the effect of  $\text{NO}_x$ ) when the dilution ratio is  $\sim 12$  (Karjalainen et al., 2016; Timonen et al., 2016). The reactions between  $\text{NO}_x$ ,  $\text{O}_3$  and OH also decrease the  $\text{OH}_{\text{exp}}$  and therefore increase the photolysis rate of VOCs. Thus, a higher dilution ratio than 12 should be used when sampling cold-start engine exhaust into the TSAR.

#### **3.4.2 Vapor losses**

To study the dependence of LVOC fate on residence time and condensational sink, we define two cases: the oxidation of ambient air (low condensational sink) and diluted vehicle exhaust (high condensational sink). The condensational sink depends on particle number concentration and size, and also on the accommodation coefficient ( $\alpha$ ), diffusion coefficient and molecular mass of the condensing vapor. The first-order rate coefficient for wall-loss ( $k_w$ ) is calculated as in Palm et al. (2016) (see Supplementary material for details on calculation of CS and  $k_w$ ). Following the example in Palm et al. (2016), we assume the following properties for the LVOC: molar mass of  $200 \text{ g mol}^{-1}$ , diffusion coefficient (D) of  $7 \times 10^{-6} \text{ m}^2 \text{ s}^{-1}$ , and  $k_{\text{OH}} = 1 \times 10^{-11} \text{ cm}^3 \text{ molec.}^{-1} \text{ s}^{-1}$ . For simplicity, we assume that the nucleation rate in Eqs. (5-7) is zero. Nucleation is still implicitly taken into account because the condensational sink is calculated from average size distribution before and after TSAR. In addition, we do not consider the heterogeneous fragmentation.

In the case of oxidation of ambient air, the timescale for condensation on aerosol  $\tau_{aer} = (4\pi \cdot D \cdot CS)^{-1} \approx 65 \text{ s}$  (when  $\alpha = 1$ ). According to Palm et al. (2016), this is a typical value for ambient pine forest air oxidized in PAM chamber, when sufficient amount of precursors are available for SOA formation. This CS is equivalent to that of a log-normal particle size distribution with total number concentration of  $1.5 \times 10^5 \text{ cm}^{-3}$ , median diameter ( $\mu$ ) of 25 nm and geometric standard deviation ( $\sigma$ ) of 1.4.

5 The use of particle size distribution instead of a constant CS allows us to vary  $\alpha$  (since CS depends on  $\alpha$ ). Different values for LVOC mass accommodation coefficients have been proposed. For example, (Saleh et al., (2013) measured a value of  $\alpha \approx 0.1$  for alpha-pinene SOA, whereas Palm et al. (2016) argue that  $\alpha \approx 1.0$  for ambient pine forest SOA.

The vapor losses in TSAR for the ambient case as a function of residence time were modeled using the method described in Sect. 2.5.2. Two values of the mass accommodation coefficients were used ( $\alpha = 0.1$  and  $\alpha = 1.0$ ). The equivalent  $\text{OH}_{\text{exp}}$  is 5 days regardless of the residence time. The results are presented in Fig. 7a. At typical TSAR residence time (37 s), the LVOC losses in this case are 69-96 %, depending on the value of  $\alpha$ . Most losses are caused by fragmentation, and longer residence time results in less losses (Fig. S5). This is because the shorter the residence time, the higher the OH concentration must be to reach the same equivalent OH exposure. When the OH concentration is high enough, the timescale of fragmentation is lower than that of condensation.

10

15

The vehicle exhaust case is based on the measurements in Sect. 3.6. The mass concentration and  $\tau_{aer}$  of diluted primary aerosol are approximately  $4.8 \mu\text{g m}^{-3}$  and  $81 \text{ s}^{-1}$ , respectively (when  $\alpha = 1$ ). This is approximated as a log-normal size distribution with  $\mu = 31 \text{ nm}$ ,  $\sigma=1.9$  and number concentration of  $5.4 \times 10^4 \text{ cm}^{-3}$ . According to the measurements in Sect. 3.6, the mass concentration after TSAR is approximately  $156 \mu\text{g m}^{-3}$  (when background is subtracted). For simplicity, we assume that the increase in mass is caused only by condensation so that number concentration and  $\sigma$  are constant. Thus, the size distribution after TSAR is otherwise similar to the primary size distribution, but  $\mu = 103 \text{ nm}$ . The average CS in TSAR is calculated from the average of these two size distributions.

20

The results for the car exhaust case are presented in Fig. 7b. Now, the LVOC losses in TSAR at typical residence time are 25-80 % depending on the value of  $\alpha$ . The losses are lower than in the ambient case because of shorter timescale of condensation caused by the higher CS. Again, the highest loss is caused by fragmentation (Fig. S5).

25

In addition to TSAR, we present the estimates for LVOC losses in several other flow reactors, namely MSC, PAM reactor, and Caltech Photooxidation Flow Tube Reactor (CPOT) (Huang et al., 2016) at their typical residence times in Fig. 7. The results differ a little from the TSAR curve because of the different surface-area-to-volume ratios. One must note that the applications of the flow reactors are different; e.g. the MSC is usually used with much higher CS than what is modeled here (e.g. Corbin et al., 2015) and consequently the losses are smaller than in Fig. 7. Similarly, the main application of the TSAR is engine exhaust measurement, where the CS is usually higher than in ambient air.

30

35

The model is tested by comparing the measured and modeled sulfuric acid losses, and the results are shown in Fig. 8. In the model, the following values are assumed for the sulfuric acid molecules: molar mass of  $98 \text{ g mol}^{-1}$ ,  $\alpha = 0.65$  (Pöschl et al., 1998) and  $D = 1 \times 10^{-5} \text{ m}^2 \text{ s}^{-1}$  (Hanson and Eisele, 2000; Palm et al., 2016). We assume there is no fragmentation for sulfuric acid molecules. The CS is again calculated from the average of size distributions after and before TSAR (in this case the size distribution after TSAR divided by two). For the three measurements with the smallest error bars, the measured sulfuric acid loss is on average 4 %. The modeled loss, in contrast, is 18 % on average. The reason for this discrepancy may be the underestimated CS, since dividing the measured size distribution by two does not necessarily represent the average size distribution in TSAR. If instead the measured size distribution is used for CS calculation (the upper limit for average CS), the

40

model results in average loss of 6 %, which is much closer to the measured one and indicates that the nucleated particles generate a high CS already during the first steps of oxidation. Thus, the modeled losses for the ambient and vehicle exhaust case are probably slightly overestimated.

- 5 The sulfuric acid experiment shows that the model predicts the losses of a non-fragmenting low-volatile compound reasonably well. However, in Fig. S5 we see that it is the fragmentation that causes the highest losses for LVOCs when the residence time is short (< 50 s). The assumption that 5 oxidation steps result in fragmentation is artificial, but if we as a sensitivity test assume that the fragmentation does not occur at all, the change in overall loss is small because a higher proportion of the LVOCs will exit the reactor before condensing (Fig. S6). Still, the losses are little lower in case of no fragmentation, and thus more studies  
10 on fragmentation are needed to verify the assumptions in the model.

The modeled cases inarguably show that there is a tradeoff between residence time and LVOC losses: the smaller the residence time, the more losses. Thus, the residence time must be chosen according to the application. If a short residence time is used and the CS is low, the injection of seed particles in the sample will reduce the LVOC losses. In the car exhaust case, the CS is  
15 high enough for TSAR if the mass accommodation coefficient of the condensing vapor is close to unity. For steady-state experiments, we recommend using a long residence time when there is no need for fast response. However, even though the LVOC losses are smallest for long-residence time reactors according to the model results, the particle losses are higher (e.g. ~20 % for PAM and CPOT for 100 nm particles, in TSAR ~0%) (Huang et al., 2016; Lambe et al., 2011).

- 20 ~~The measured sulfuric acid mass as a function of expected mass is shown in Fig. 6. For the three measurements with the smallest error bars, the measured mass is on average 4 % lower than the expected mass, indicating that there are no significant losses of sulfuric acid vapor or particles.~~

### 3.5 Toluene SOA yield and properties

The SOA formation studies were conducted as described in Sect. 2.6. Toluene concentration in the sample entering the reactors  
25 was 320 ppb ( $\pm 34$  ppb). During the experiments, ~~The~~the average temperature of sample was ~~23—24~~ $23.6 \pm 0.2$  °C and the average relative humidity ~~26—34~~ $31.3 \pm 2.9$  %, where the uncertainty is the standard deviation of the values. ~~with the exception of the PAM measurement at highest OH exposure, where the average relative humidity was 37 %.~~

#### 3.5.1 Steady state experiments

The SOA mass formed in the reactors is calculated from the number size distribution measured by the SMPS, assuming  
30 spherical particles with a density of  $1.45 \text{ g cm}^{-3}$  (Ng et al. 2007). The SMPS was used for PM concentration measurements instead of the AMS because especially for the TSAR, all particles do not fall in the AMS detection range (40 nm–800 nm). The background mass, i.e. the mass formed in the reactors in the absence of toluene, was subtracted from the toluene SOA mass. The background mass consists of oxidation products of the dilution air, and depends on the purity of the pressurized air. The purity of the air must be always checked by measuring the mass formed in the flow reactor in absence of any exhaust or  
35 precursors. In this experiment, the background mass concentration was on average  $1.2 \mu\text{g m}^{-3}$  for the TSAR and  $1.1 \mu\text{g m}^{-3}$  for the PAM. For comparison, the average mass concentration in toluene measurements was  $137 \mu\text{g m}^{-3}$ .

Figure ~~7~~9 shows SMPS mass distributions of toluene SOA for PAM and TSAR at  $\text{OH}_{\text{exp}}$  of ~~1.33.6~~ $1.336 \times 10^{12}$  molec. s  $\text{cm}^{-3}$  and ~~6.04.1~~ $6.041 \times 10^{121}$  molec. s  $\text{cm}^{-3}$ , respectively. The PAM produces a wide mass distribution where particles above 100 nm contribute to approximately half of the total mass. The TSAR produces a narrower mass distribution where approximately half of total mass is located in particles smaller than 40 nm. This phenomenon was also reported by Bruns et al. (2015): the micro-

40

smog chamber, which is smaller, has a shorter residence time, and generates smaller particles than PAM. As discussed in sections 2.5.2 and 3.4.2, the shorter residence time limits the condensational growth of particles and may favor nucleation instead of condensation. Implementing nucleation in the LVOC fate model remains a future task, but an estimation of the losses of toluene oxidation products was conducted in a similar way as in Sect. 3.4.2. If the accommodation coefficient of the oxidation products is one, the LVOC losses for the toluene SOA cases are less than 2 % except for TSAR measurement at  $\text{OH}_{\text{exp}}$  of  $3 \times 10^{10}$  molec. s  $\text{cm}^{-3}$ , where the losses are approximately 8 %. If the accommodation coefficient is 0.1, the losses are less than 35 % except for the TSAR low  $\text{OH}_{\text{exp}}$  measurement, where the losses are approximately 73 %. Since the exact value of the accommodation coefficient is unknown, the results in this section are not corrected with the estimated losses.

10 Figure 8-10 shows toluene SOA yield obtained in steady state experiments as a function of  $\text{OH}_{\text{exp}}$  for both reactors. The  $\text{OH}_{\text{exp}}$  was not measured simultaneously but is obtained as a function of  $\text{O}_3$  measured after the reactors from the model described in Sect. 2.4, assuming an  $\text{OHR}_{\text{ext}}$  equivalent to 320 ppb of toluene, and  $\pm 20$  % uncertainty in TSAR  $\text{OH}_{\text{exp}}$  and  $\pm 30$  % in PAM  $\text{OH}_{\text{exp}}$  (PAM model fitting results are presented in Fig. S7). Following the reasoning in (Peng et al., (2015), we use  $\text{SO}_2$  as a proxy for the toluene in the model. ~~the off-line calibrations.~~The maximum yield is approximately 0.2 for both reactors

15 (neglecting the TSAR outlier at  $\text{OH}_{\text{exp}}$  of  ~~$1 \times 10^{12}$~~   $6.3 \times 10^{11}$  molec. s  $\text{cm}^{-3}$  and uncertain PAM values at low  $\text{OH}_{\text{exp}}$ ), and both reactors reach the maximum yield at  $\text{OH}_{\text{exp}}$  between  $0.35 \times 10^{12}$  molec. s  $\text{cm}^{-3}$  and  $1.50 \times 10^{12}$  molec. s  $\text{cm}^{-3}$ . However, the TSAR yield is more sensitive to  $\text{OH}_{\text{exp}}$  than the PAM yield. One possible reason is that because of the broad residence time distribution, the PAM always outputs SOA with both high and low  $\text{OH}_{\text{exp}}$  regardless of the mean  $\text{OH}_{\text{exp}}$ . This mixing of different aged SOA may stabilize the output and reduce the sensitivity to  $\text{OH}_{\text{exp}}$ . Even higher yields are observed in PAM at

20 low  $\text{OH}_{\text{exp}}$  ( $< 3 \times 10^{11}$  molec. s  $\text{cm}^{-3}$ ), but the calculation of yield at this low  $\text{OH}_{\text{exp}}$  is very sensitive, because of the small value of the denominator in Eq. (17). This is seen as high uncertainty in PAM yields at low  $\text{OH}_{\text{exp}}$ . The uncertainty highlights the importance of simultaneous, accurate measurement of  $\text{OH}_{\text{exp}}$  especially when the PAM light intensity is low. At higher  $\text{OH}_{\text{exp}}$  the yields of the two reactors agree very well.

25 When the  $\text{OH}_{\text{exp}}$  is higher than  $1 \times 10^{12}$  molec. s  $\text{cm}^{-3}$ , the yield starts to decrease in both reactors. This indicates that the assumption on fragmentation in the LVOC loss model (Sect. 2.5.2) is right: the higher the OH concentration, the more fragmentation occurs. The fragmented molecules will not condense on aerosol phase and thus the yield is lower. Still, these results cannot be used to validate the simplified model assumption that 5 oxidation steps of an LVOC leads to fragmentation.

30 The PAM yield in Fig. 10 is not corrected for particle losses, because the losses are characterized only for particles that enter the PAM at certain size and do not grow inside the PAM by condensation. This is not the case here, because the particles are formed via nucleation inside the PAM, and thus it is unknown how long they have spent in the reactor and what is the particle size as a function of residence time. As an estimate, the particle size-distribution measured after PAM was corrected with the losses measured for this particular chamber (Karjalainen et al., 2016). With this correction, the PAM yield would increase by

35 19 % on average.

Kang et al. (2007) reported a toluene SOA yield of 0.09 using an early version of the PAM at similar relative humidity, temperature and toluene concentration as in this paper. Ng et al. (2007) and Hildebrandt et al. (2009) used smog chambers with seed particles and low relative humidity, and reported toluene SOA yields of 0.30 and 0.26-0.41, respectively. The SOA yield in this study is therefore slightly lower than in smog chamber studies, which may be caused by the lack of seed particles: Lambe et al. (2015) showed that the addition of seed particles in the PAM resulted in a higher SOA yield, at least in the case of isoprene.

In addition to yield, the chemical composition of produced SOA was studied. In Fig. 911, a van Krevelen diagram shows the oxidation state of SOA for both reactors. In this diagram, H/C ratio is shown as a function of O/C ratio. Elemental ratios are calculated using the method developed by Aiken et al. (2008) and improved by Canagaratna et al. (2015). Oxidation of aerosol usually increases the O/C ratio and decreases the H/C ratio (Heald et al., 2010). This phenomenon is observed in both reactors, and based on these ratios, the oxidation state of SOA is similar in PAM and TSAR at comparable OH exposures, ~~when the exposure is less than 7 equivalent days. At higher OH<sub>exp</sub>, similar ratios are still observed in both reactors, but at different OH exposures.~~

10 To further compare the SOA oxidation state in the reactors, the average carbon oxidation state ( $\overline{OS}_C$ ) of SOA is shown in Fig. ~~1012~~. The average carbon oxidation state is a metric which is invariant to hydration or dehydration, and is defined as  $\overline{OS}_C \approx 2 \times O/C - H/C$  (Canagaratna et al., 2015; Kroll et al., 2011). As well as the O/C ratios and H/C ratios, the  $\overline{OS}_C$  of the SOA in the reactors also agree at comparable OH<sub>exp</sub>. differ at high OH<sub>exp</sub>. The TSAR SOA has higher oxidation state than the PAM SOA even though the OH<sub>exp</sub> is similar. The trend of TSAR and PAM  $\overline{OS}_C$  as a function of OH<sub>exp</sub> seems to differ at higher OH<sub>exp</sub>, but this can be caused by the uncertainty in the OH<sub>exp</sub> estimation, which is visualized with error bars in Fig. 12.

~~These discrepancies in the oxidation state suggest that the OH<sub>exp</sub> alone does not affect the composition of SOA. For example, in Fig. 10 the  $\overline{OS}_C$  of TSAR SOA increases from 0.32 to 0.63 even though the increase in OH<sub>exp</sub> is small ( $2.0 \times 10^{11}$  molec. s cm<sup>-3</sup>). PAM SOA needs an increase of  $4.0 \times 10^{11}$  molec. s cm<sup>-3</sup> in OH<sub>exp</sub> to achieve the same increase in  $\overline{OS}_C$  (from 0.34 to 0.63). The difference between TSAR and PAM in the high  $\overline{OS}_C$  region is that the outlet ozone concentration in TSAR increases by 42 ppm when OH<sub>exp</sub> increases by  $5.1 \times 10^{11}$  molec. s cm<sup>-3</sup>, whereas in PAM the outlet ozone concentration increases only by 7.2 ppm at comparable change in OH<sub>exp</sub> ( $6.4 \times 10^{11}$  molec. s cm<sup>-3</sup>). Thus, the increasing ozone exposure in TSAR may lead to the increase in  $\overline{OS}_C$ , which suggests that the toluene oxidation products react with ozone. However, also the OH<sub>exp</sub> estimation may be uncertain, since it is based on off line calibration. In this experiment, the high concentration of toluene likely decreases the OH<sub>exp</sub>, and this effect may have a different magnitude between the reactors. This could also explain the discrepancies in Fig. 10.~~

We also compare ~~The~~ the chemical composition of SOA ~~is further compared~~ by studying the organic mass spectra. According to Marcolli et al. (2006) and Lambe et al. (2015), a dot product between two normalized mass spectra can be used to determine whether the spectra are similar. The spectra are normalized by dividing each signal by the square root of the sum of the squares of all signals. A dot product of one implicates that the spectra are identical, and zero that they are orthogonal.

Toluene SOA here is divided in three categories: low oxidation ( $-0.18 < \overline{OS}_C < -0.16$ ), medium oxidation ( $0.50 < \overline{OS}_C < 0.69$ ) and high oxidation ( $\overline{OS}_C > 1.10$ ). The dot products between the organic spectra of different reactors are shown in Table 2. The dot products of normalized mass spectra of SOA produced in reactors at comparable  $\overline{OS}_C$  are above 0.99, indicating that the reactors produce similar SOA matter in regard to chemical composition.

The TSAR and PAM reactors differ in volume, geometry, flow conditions and residence time. The most significant difference is in the oxidation process: TSAR operates in OFR254 mode and PAM in OFR185 mode. However, the agreement between yields and organic mass spectra of SOA produced in both the TSAR and PAM reactors show that the oxidation products are similar in both reactors, at least in the case of toluene. In OFR254, the sample is first exposed to ozone (before the oxidation reactor) and then to both ozone and OH radicals. If the VOCs in the sample react fast with ozone, resulting SOA mass might differ between OFR254 and OFR185. This was not the case for toluene, as dark experiments (only ozone, no UV light) did

not produce any secondary mass. In other applications, for example when oxidizing biogenic precursors which are highly reactive towards ozone, the results between OFR254 and OFR185 presumably differ, OFR185 being more realistic as the sample is exposed to ozone and OH simultaneously. However, the main application of TSAR is to measure vehicle emissions, which are more reactive towards OH than ozone (Gentner et al., 2012; Tkacik et al., 2014). The potential of ozone to produce SOA from the emission can be measured by injecting ozone into the TSAR with UV lights turned off.

### 3.5.2 Pulse experiments

The SOA mass concentrations as a function of time are shown in Fig. ~~11~~13 for all pulse experiments. The 10 s pulse of toluene results in a sharp peak in mass in the TSAR, whereas the PAM reactor produces significantly broader peaks at both used flow rates. Interestingly, the TSAR mass peak is divided into two distinct peaks. We do not know the reason for this phenomenon since the residence time distributions in Sect 3.1 do not support this kind of behavior. However, the flow conditions in this experiment are not exactly the same as in Sect 3.1: here, the flow rate in residence time chamber is only 10 slpm, whereas in Sect. 3.1 it was 50 slpm.

Cycle 1 with three rapid toluene pulses shows the importance of laminar flow and short residence time in TSAR: PAM produces only one broad peak whereas all the three pulses can be distinguished in the SOA mass produced by the TSAR. In cycle 2, where toluene pulses are injected between longer intervals, the pulses are also separated in the mass produced by PAM.

As the total amount of toluene injected into the reactors is known and the yield is determined in Sect. 3.5.1, the total mass produced in the reactors can be predicted with Eq. (~~12~~23).

$$M_{predicted} = M_{tol} \times Y, \quad (1223)$$

where  $M_{tol}$  is the total mass of the toluene injected and  $Y$  is the yield. In these experiments, the  $OH_{exp}$  was approximately  $0.9 \times 10^{12} \pm 6.1 \times 10^{11}$  molec. s  $cm^{-3}$  in TSAR and  $1.3 \times 10^{12} \pm 8.3 \times 10^{11}$  molec. s  $cm^{-3}$  in PAM, so a yield of 0.2 is used for both reactors to calculate the expected mass. The mass produced in the reactors is the area of the peaks in Fig. ~~10~~13 multiplied by the flow rate through the reactors. The comparison between the expected mass and the formed mass is shown in Fig. ~~12~~14.

In all the experiments, the mass produced in the reactors agree well with the expected mass. For the 10 s pulse, PAM mass is lower than the expected mass and TSAR mass; for cycle 1, TSAR produces more mass than expected; and for cycle 2, both reactors produce less mass than predicted. Considering the uncertainties in this experiment, namely the dilution ratio, EEPS inversion and toluene concentration, we conclude there are no significant differences in the total mass the reactors produce, even though the pulse shapes are clearly different. In all the cases, the mass produced in PAM is slightly lower than in TSAR, probably because the particle losses in PAM are higher.

The agreement between the predicted mass and the produced mass suggest that the approach to measure the secondary aerosol formation potential in real-time is valid: the narrow residence time distribution of TSAR gives time-resolved information of SOA formation from fast changing precursor concentrations but still produces approximately the same amount of mass as the PAM reactor, where the oxidation process is slower. Based on these results and the LVOC loss estimation in Sect. 3.4.2, this holds when the condensational sink is high enough. When the CS is smaller (e.g. in ambient air measurements), we expect that the TSAR produces less mass than the PAM due to the higher losses.-

### 3.6 Engine exhaust oxidation

When measuring time-resolved secondary aerosol formation during a transient driving cycle, it is crucial to synchronize real-time aerosol measurements with vehicle speed data. This is performed by comparing the CO<sub>2</sub> measurements in tailpipe and after the dilution steps.

#### 5 3.6.1 TSAR oxidation

In Sect. 3.3 we showed that the OH<sub>exp</sub> in TSAR depends on relative humidity and ozone concentration. In engine exhaust experiments RH was 33-36 % and temperature 22 °C. Ozone concentration was not measured but based on later laboratory experiments, the ozone concentration has been approximately 11 ppm in the sample flow. According to the results presented in Sect. 3.3, the OH<sub>exp</sub> with this ozone concentration is approximately  $8 \times 10^{11}$  molec. s cm<sup>-3</sup> (equivalent photochemical age of 6.3 days). However, this should be considered only as an upper limit for the OH<sub>exp</sub>. There is always NO present in the exhaust sample, and the ozone reacts fast with NO, titrating practically all NO to NO<sub>2</sub> before the sample enters the TSAR. Therefore, NO emissions cause a loss in ozone concentration, suppressing the OH<sub>exp</sub>. In addition, NO<sub>2</sub> and other OH reactive compounds in the exhaust further decrease the OH<sub>exp</sub>. As the concentrations of NO<sub>x</sub> and other gaseous compounds vary during the driving cycle, so does the OH<sub>exp</sub>. The time resolved OH<sub>exp</sub> during the driving cycle should be determined by monitoring an OH reactive tracer, such as CO. In this work, the OH<sub>exp</sub> was not measured in real-time.

#### 3.6.2 Time-resolved secondary aerosol formation

The secondary aerosol mass concentration formed from the GDI exhaust during a warm NEDC is shown in Fig. 15c. Mass concentration is calculated from particle number size distribution measured by EEPS assuming spherical particles with a density of 1.0 g cm<sup>-3</sup> and multiplying the result by the total dilution ratio. The shown mass concentration is an average value of two identical warm NEDCs, and the standard deviation between these two measurements is shown as shaded area. A constant value of background mass formed from dilution air has been subtracted from the calculated mass. Because of the background mass, the vapor losses here are lower than those modeled in Sect. 3.4.2, less than 2 % if the accommodation coefficient is 1.0.

Figure 15c shows significant differences in secondary aerosol formation during different driving conditions. The small standard deviation suggests that the operation of TSAR and the phenomena causing secondary aerosol formation are highly reproducible. The least secondary aerosol formation occurs during long steady state driving, such as the one at 70 km h<sup>-1</sup> at the end of the cycle. When the car is accelerated to 100 km h<sup>-1</sup> and to 120 km h<sup>-1</sup> at the end of the cycle, the secondary aerosol mass formation increases. During most of the cycle, the secondary mass concentration in TSAR is 10-100 times the primary mass concentration (Fig. 15b). However, the difference between primary and secondary emission factors is not that high.

The time-resolved emission factor of secondary aerosol mass in Fig. 15c is achieved by multiplying the secondary mass concentration by the exhaust mass flow. Low exhaust mass flow during engine braking cancels out the high mass concentration peaks. Instead, the peak at the end of the cycle dominates the emissions of secondary aerosol precursors. The total emission factor over the cycle is the integral of the time-resolved emission factor over the cycle length divided by the total distance. For the primary emissions, the emission factor is 0.1 mg km<sup>-1</sup> and for the secondary aerosol potential 25 times higher, 2.7 mg km<sup>-1</sup>.

The secondary aerosol emission factors for a similar vehicle and driving cycle reported by (Karjalainen et al., (2016) and (Platt et al., (2013) are 4.3 mg km<sup>-1</sup> and 12.7 mg km<sup>-1</sup> (SOA only), respectively. The values are higher than in this study, possibly because the OH exposures are different: using a PAM reactor, (Tkacik et al., (2014) have shown that the SOA formation from

vehicle exhaust depends strongly on the OH exposure. Another reason for the higher values is probably that both Karjalainen et al. (2016) and Platt et al. (2013) used a cold-start cycle. In Karjalainen et al. (2016), most of the secondary mass is indeed formed in the beginning of the cycle, when the engine and the after-treatment system are cold. Interestingly, Karjalainen et al. (2016) do not observe a similar peak in the secondary mass formation at the end of the cycle as we see in Fig. 15c. However, the gas measurements by Karjalainen et al. (2016) and Platt et al. (2013) show that during the last acceleration in the cycle, there are elevated concentrations of total hydrocarbons and ammonia, which could be potential sources of SOA and ammonium nitrate formation in an oxidation flow reactor.

We also observe a new phenomenon, where engine braking results in high concentrations of secondary aerosol forming precursors. Every deceleration (i.e. engine braking) during warm NEDC produces a peak in secondary mass concentration. The tail at the beginning of the cycle is also a result from engine braking, as steady-state driving at 80 km h<sup>-1</sup> was always performed before the warm NEDC. This phenomenon is not evident in the results of Karjalainen et al. (2016), since the mass concentration does not seem to correlate with vehicle speed in their study. However, they observe repeated events of nanoparticle growth in the PAM during the cycle, which could be related to engine braking. Because of the mixing of the sample inside the PAM, it is impossible to link these growth events to certain phases in the driving cycle.

~~The time-resolved emission factor of secondary aerosol mass in Fig. 13 is achieved by multiplying the secondary mass concentration by the exhaust mass flow. Low exhaust mass flow during engine braking cancels out the high mass concentration peaks. Instead, the peak at the end of the cycle dominates the emissions of secondary aerosol precursors.~~

Since no aerosol chemical composition measurements were performed, we cannot specify the amount of organic mass in the formed secondary aerosol, and therefore we do not present the emission factor for SOA potential of the engine exhaust. In addition, the high background mass (i.e. unclean dilution air) and the lack of real-time OH<sub>exp</sub> measurement make this data qualitative rather than quantitative. However, this experiment shows the feasibility of TSAR to measure the time-resolved secondary aerosol formation potential of rapidly changing vehicle emissions. This way, we can identify the driving conditions in which most secondary aerosol forming precursors are emitted. If the sample was injected to a smog chamber with a constant dilution ratio and then oxidized, like Platt et al. (2013) did, the precursor pulses emitted during engine braking events would cause an over-estimation of total secondary aerosol formation potential.

#### 4 Conclusions

In this work, we introduced TSAR, a new short-residence-time oxidation flow reactor for secondary aerosol formation studies measurements. We studied the performance of the reactor by measuring the sulfuric acid yield, toluene SOA yield as well as the composition and the secondary aerosol formation potential of light-duty gasoline vehicle exhaust during a transient driving cycle. In addition, we characterized the particle transmission efficiency and the residence time distribution of the reactor and did a modeling study on vapor losses in TSAR-

According to the model results, the vapor losses in TSAR are higher than in the reactors with longer residence times. The losses depend strongly on the condensational sink of the sample, which is usually high in exhaust measurements (resulting in lower losses). For applications with low condensational sink, we recommend longer residence time than in the TSAR or injection of seed aerosol. When there is no possibility for seed aerosol injection, a tradeoff must be made between fast response and low vapor losses.

The toluene experiments show that both SOA yield and composition are similar in TSAR SOA as in PAM SOA, even though PAM operates in OFR185 mode and TSAR in OFR254 mode. The similarity indicates that the TSAR can be used instead of the OFR185 PAM reactor when high time-resolution is needed. is able to simulate atmospheric SOA formation since Bruns et al. (2015) and Lambe et al. (2015) show that the composition of SOA formed in PAM is similar to the SOA formed in a smog chamber.

The particle losses in TSAR are negligible and the flow is near-laminar. These properties, together with short residence time, make TSAR better suited for monitoring the secondary aerosol formation potential of rapidly changing emission sources than the PAM chamber. We demonstrate the importance of this feature by measuring the secondary aerosol formation of car exhaust during a driving cycle. This experiment shows that TSAR is able to differentiate which driving conditions are most significant regarding the secondary aerosol formation potential.

## 5 Data availability

The data of this study is available from the authors upon request.

## 6 Acknowledgements

The TSAR was designed and built in the project “Finnish-Chinese Green ICT R&D&I Living Lab for Energy Efficient, Clean and Safe Environments”, financially supported by Finnish Funding Agency for Innovation (Tekes), and Ahlstrom Oy, FIAC Invest Oy, Green Net Finland Oy, Kauriala Oy, Lassila & Tikanoja Oyj, Lifa Air Oy, MX Electrix Oy, Pegasor Oy and Sandbox Oy.

The TSAR characterization was conducted in the framework of the HERE project funded by Tekes (the Finnish Funding Agency for Innovation), Agco Power Oy, Dinex Ecocat Oy, Dekati Oy, Neste Oyj, Pegasor Oy and Wärtsilä Finland Oy.

Pauli Simonen acknowledges Tampere University of Technology Graduate School.

## 25 References

- Aiken, A. C., DeCarlo, P. F., Kroll, J. H., Worsnop, D. R., Huffman, J. A., Docherty, K. S., Ulbrich, I. M., Mohr, C., Kimmel, J. R., Sueper, D., Sun, Y., Zhang, Q., Trimborn, A., Northway, M., Ziemann, P. J., Canagaratna, M. R., Onasch, T. B., Alfarra, M. R., Prevot, A. S. H., Dommen, J., Duplissy, J., Metzger, A., Baltensperger, U. and Jimenez, J. L.: O/C and OM/OC Ratios of Primary, Secondary, and Ambient Organic Aerosols with High-Resolution Time-of-Flight Aerosol Mass Spectrometry, *Environ. Sci. Technol.*, 42(12), 4478–4485, doi:10.1021/es703009q, 2008.
- Arffman, A., Yli-Ojanperä, J., Kalliokoski, J., Harra, J., Pirjola, L., Karjalainen, P., Rönkkö, T. and Keskinen, J.: High-resolution low-pressure cascade impactor, *J. Aerosol Sci.*, 78, 97–109, doi:10.1016/j.jaerosci.2014.08.006, 2014.
- Atkinson, R.: Kinetics and mechanisms of the gas-phase reactions of the hydroxyl radical with organic compounds under atmospheric conditions, *Chem. Rev.*, 85, 69–201, doi:10.1021/cr00071a004, 1985.
- Brockmann, J. E.: Aerosol Transport in Sampling Lines and Inlets, in *Aerosol Measurement - Principles, Techniques and Applications*, edited by P. Kulkarni and P. A. Baron, John Wiley & Sons, Inc., New Jersey., 2011.
- Bruns, E. A., El Haddad, I., Keller, A., Klein, F., Kumar, N. K., Pieber, S. M., Corbin, J. C., Slowik, J. G., Brune, W. H., Baltensperger, U. and Prévôt, A. S. H.: Inter-comparison of laboratory smog chamber and flow reactor systems on

- organic aerosol yield and composition, *Atmos. Meas. Tech.*, 8(6), 2315–2332, doi:10.5194/amt-8-2315-2015, 2015.
- Canagaratna, M. R., Jimenez, J. L., Kroll, J. H., Chen, Q., Kessler, S. H., Massoli, P., Hildebrandt Ruiz, L., Fortner, E., Williams, L. R., Wilson, K. R., Surratt, J. D., Donahue, N. M., Jayne, J. T. and Worsnop, D. R.: Elemental ratio measurements of organic compounds using aerosol mass spectrometry: Characterization, improved calibration, and implications, *Atmos. Chem. Phys.*, 15(1), 253–272, doi:10.5194/acp-15-253-2015, 2015.
- Corbin, J. C., Keller, A., Lohmann, U., Burtscher, H., Sierau, B. and Mensah, A. A.: Organic Emissions from a Wood Stove and a Pellet Stove Before and After Simulated Atmospheric Aging, *Aerosol Sci. Technol.*, 49(11), 1037–1050, doi:10.1080/02786826.2015.1079586, 2015.
- Fogler, H. S.: *Elements of Chemical Reaction Engineering*, Prentice Hall PTR., 2006.
- Gentner, D. R., Isaacman, G., Worton, D. R., Chan, A. W. H., Dallmann, T. R., Davis, L., Liu, S., Day, D. A., Russell, L. M., Wilson, K. R., Weber, R., Guha, A. and Harley, R. A.: Elucidating secondary organic aerosol from diesel and gasoline vehicles through detailed characterization of organic carbon emissions, , doi:10.1073/pnas.1212272109/-/DCSupplemental.www.pnas.org/cgi/doi/10.1073/pnas.1212272109, 2012.
- Hanson, D. R. and Eisele, F.: Diffusion of H<sub>2</sub>SO<sub>4</sub> in Humidified Nitrogen: Hydrated H<sub>2</sub>SO<sub>4</sub>, *J. Phys. Chem. A*, 104(8), 1715–1719, doi:10.1021/jp993622j, 2000.
- Harra, J., Mäkitalo, J., Siikanen, R., Virkki, M., Genty, G., Kobayashi, T., Kauranen, M. and Mäkelä, J. M.: Size-controlled aerosol synthesis of silver nanoparticles for plasmonic materials, *J. Nanoparticle Res.*, 14(6), 870, doi:10.1007/s11051-012-0870-0, 2012.
- Heald, C. L., Kroll, J. H., Jimenez, J. L., Docherty, K. S., Decarlo, P. F., Aiken, A. C., Chen, Q., Martin, S. T., Farmer, D. K. and Artaxo, P.: A simplified description of the evolution of organic aerosol composition in the atmosphere, *Geophys. Res. Lett.*, 37(8), doi:10.1029/2010GL042737, 2010.
- Huang, Y., Coggon, M. M., Zhao, R., Lignell, H., Bauer, M. U., Flagan, R. C. and Seinfeld, J. H.: The Caltech Photooxidation Flow Tube Reactor - I: Design and Fluid Dynamics, *Atmos. Meas. Tech. Discuss.*, (September), 1–36, doi:10.5194/amt-2016-282, 2016.
- Johnson, T., Caldow, R., Pocher, A., Mirmem, A. and Kittelson, D.: A New Electrical Mobility Particle Sizer Spectrometer for Engine Exhaust Particle Measurements, in SAE paper, vol. 2004-01-13., 2004.
- Kanakidou, M., Seinfeld, J. H., Pandis, S. N., Barnes, I., Dentener, F. J., Facchini, M. C., Van Dingenen, R., Ervens, B., Nenes, A., Nielsen, C. J., Swietlicki, E., Putaud, J. P., Balkanski, Y., Fuzzi, S., Horth, J., Moortgat, G. K., Winterhalter, R., Myhre, C. E. L., Tsigaridis, K., Vignati, E., Stephanou, E. G. and Wilson, J.: Organic aerosol and global climate modelling: a review, *Atmos. Chem. Phys.*, 5(4), 1053–1123, doi:10.5194/acp-5-1053-2005, 2005.
- Kang, E., Root, M. J., Toohey, D. W. and Brune, W. H.: Introducing the concept of Potential Aerosol Mass (PAM), *Atmos. Chem. Phys.*, 7(22), 5727–5744, doi:10.5194/acp-7-5727-2007, 2007.
- Karjalainen, P., Timonen, H., Saukko, E., Kuuluvainen, H., Saarikoski, S., Aakko-Saksa, P., Murtonen, T., Bloss, M., Dal Maso, M., Simonen, P., Ahlberg, E., Svenningsson, B., Brune, W. H., Hillamo, R., Keskinen, J. and Rönkkö, T.: Time-resolved characterization of primary particle emissions and secondary particle formation from a modern gasoline passenger car, *Atmos. Chem. Phys.*, 16(13), 8559–8570, doi:10.5194/acp-16-8559-2016, 2016.
- Keller, A. and Burtscher, H.: A continuous photo-oxidation flow reactor for a defined measurement of the SOA formation potential of wood burning emissions, *J. Aerosol Sci.*, 49, 9–20, doi:10.1016/j.jaerosci.2012.02.007, 2012.
- Keskinen, J. and Rönkkö, T.: Can real-world diesel exhaust particle size distribution be reproduced in the laboratory? A critical review., *J. Air Waste Manag. Assoc.*, 60(October), 1245–1255, doi:10.3155/1047-3289.60.10.1245, 2010.
- Kroll, J. H., Smith, J. D., Che, D. L., Kessler, S. H., Worsnop, D. R. and Wilson, K. R.: Measurement of fragmentation and functionalization pathways in the heterogeneous oxidation of oxidized organic aerosol, *Phys. Chem. Chem. Phys.*, 11, 8005–8014, doi:10.1039/b916865f, 2009.

- Kroll, J. H., Donahue, N. M., Jimenez, J. L., Kessler, S. H., Canagaratna, M. R., Wilson, K. R., Altieri, K. E., Mazzoleni, L. R., Wozniak, A. S., Bluhm, H., Mysak, E. R., Smith, J. D., Kolb, C. E. and Worsnop, D. R.: Carbon oxidation state as a metric for describing the chemistry of atmospheric organic aerosol., *Nat. Chem.*, 3(2), 133–139, doi:10.1038/nchem.948, 2011.
- 5 Lambe, A. T., Ahern, A. T., Williams, L. R., Slowik, J. G., Wong, J. P. S., Abbatt, J. P. D., Brune, W. H., Ng, N. L., Wright, J. P., Croasdale, D. R., Worsnop, D. R., Davidovits, P. and Onasch, T. B.: Characterization of aerosol photooxidation flow reactors: heterogeneous oxidation, secondary organic aerosol formation and cloud condensation nuclei activity measurements, *Atmos. Meas. Tech.*, 4(3), 445–461, doi:10.5194/amt-4-445-2011, 2011.
- 10 Lambe, A. T., Chhabra, P. S., Onasch, T. B., Brune, W. H., Hunter, J. F., Kroll, J. H., Cummings, M. J., Brogan, J. F., Parmar, Y., Worsnop, D. R., Kolb, C. E. and Davidovits, P.: Effect of oxidant concentration, exposure time, and seed particles on secondary organic aerosol chemical composition and yield, *Atmos. Chem. Phys.*, 15(6), 3063–3075, doi:10.5194/acp-15-3063-2015, 2015.
- 15 Li, R., Palm, B. B., Ortega, A. M., Hlywiak, J., Hu, W., Peng, Z., Day, D. A., Knote, C., Brune, W. H., de Gouw, J. A. and Jimenez, J. L.: Modeling the Radical Chemistry in an Oxidation Flow Reactor: Radical Formation and Recycling, Sensitivities, and the OH Exposure Estimation Equation, *J. Phys. Chem. A*, 119(19), 4418–4432, doi:10.1021/jp509534k, 2015.
- Mao, J., Ren, X., Brune, W. H., Olson, J. R., Crawford, J. H., Fried, A., Huey, L. G., Cohen, R. C., Heikes, B., Singh, H. B., Blake, D. R., Sachse, G. W., Diskin, G. S., Hall, S. R. and Shetter, R. E.: Airborne measurement of OH reactivity during INTEX-B, *Atmos. Chem. Phys.*, 9(1), 163–173, doi:10.5194/acp-9-163-2009, 2009.
- 20 Marcolli, C., Canagaratna, M. R., Worsnop, D. R., Bahreini, R., de Gouw, J. a., Warneke, C., Goldan, P. D., Kuster, W. C., Williams, E. J., Lerner, B. M., Roberts, J. M., Meagher, J. F., Fehsenfeld, F. C., Marchewka, M. L., Bertman, S. B. and Middlebrook, a. M.: Cluster analysis of the organic peaks in bulk mass spectra obtained during the 2002 New England Air Quality Study with an Aerodyne aerosol mass spectrometer, *Atmos. Chem. Phys. Discuss.*, 6(3), 4601–4641, doi:10.5194/acpd-6-4601-2006, 2006.
- 25 Odum, J. R., Hoffmann, T., Bowman, F., Collins, D., Flagan, R. C. and Seinfeld, J. H.: Gas/Particle Partitioning and Secondary Organic Aerosol Yields, *Environ. Sci. Technol.*, 30(8), 2580–2585, doi:10.1021/es950943+, 1996.
- Onasch, T. B., Trimborn, a., Fortner, E. C., Jayne, J. T., Kok, G. L., Williams, L. R., Davidovits, P. and Worsnop, D. R.: Soot Particle Aerosol Mass Spectrometer: Development, Validation, and Initial Application, *Aerosol Sci. Technol.*, 46(7), 804–817, doi:10.1080/02786826.2012.663948, 2012.
- 30 Ortega, A. M., Hayes, P. L., Peng, Z., Palm, B. B., Hu, W., Day, D. A., Li, R., Cubison, M. J., Brune, W. H., Graus, M., Warneke, C., Gilman, J. B., Kuster, W. C., de Gouw, J., Gutiérrez-Montes, C. and Jimenez, J. L.: Real-time measurements of secondary organic aerosol formation and aging from ambient air in an oxidation flow reactor in the Los Angeles area, *Atmos. Chem. Phys.*, 16(11), 7411–7433, doi:10.5194/acp-16-7411-2016, 2016.
- 35 Palm, B. B., Campuzano-Jost, P., Ortega, A. M., Day, D. A., Kaser, L., Jud, W., Karl, T., Hansel, A., Hunter, J. F., Cross, E. S., Kroll, J. H., Peng, Z., Brune, W. H. and Jimenez, J. L.: In situ secondary organic aerosol formation from ambient pine forest air using an oxidation flow reactor, *Atmos. Chem. Phys.*, 16(5), 2943–2970, doi:10.5194/acp-16-2943-2016, 2016.
- Peng, C.-Y., Lan, C.-H. and Yang, C.-Y.: Effects of biodiesel blend fuel on volatile organic compound (VOC) emissions from diesel engine exhaust, *Biomass and Bioenergy*, 36, 96–106, doi:10.1016/j.biombioe.2011.10.016, 2012.
- 40 Peng, Z., Day, D. A., Stark, H., Li, R., Lee-Taylor, J., Palm, B. B., Brune, W. H. and Jimenez, J. L.: HOx radical chemistry in oxidation flow reactors with low-pressure mercury lamps systematically examined by modeling, *Atmos. Meas. Tech.*, 8(11), 4863–4890, doi:10.5194/amt-8-4863-2015, 2015.
- Peng, Z., Day, D. A., Ortega, A. M., Palm, B. B., Hu, W., Stark, H., Li, R., Tsigaridis, K., Brune, W. H. and Jimenez, J. L.:

Non-OH chemistry in oxidation flow reactors for the study of atmospheric chemistry systematically examined by modeling, *Atmos. Chem. Phys.*, 16(7), 4283–4305, doi:10.5194/acp-16-4283-2016, 2016.

- Platt, S. M., El Haddad, I., Zardini, a. a., Clairotte, M., Astorga, C., Wolf, R., Slowik, J. G., Temime-Roussel, B., Marchand, N., Ježek, I., Drinovec, L., Močnik, G., Möhler, O., Richter, R., Barmet, P., Bianchi, F., Baltensperger, U. and Prévôt, a. S. H.: Secondary organic aerosol formation from gasoline vehicle emissions in a new mobile environmental reaction chamber, *Atmos. Chem. Phys.*, 13(18), 9141–9158, doi:10.5194/acp-13-9141-2013, 2013.
- Pöschl, U., Canagaratna, M., Jayne, J. T., Molina, L. T., Worsnop, D. R., Kolb, C. E. and Molina, M. J.: Mass Accommodation Coefficient of H<sub>2</sub>SO<sub>4</sub> Vapor on Aqueous Sulfuric Acid Surfaces and Gaseous Diffusion Coefficient of H<sub>2</sub>SO<sub>4</sub> in N<sub>2</sub>/H<sub>2</sub>O, *J. Phys. Chem. A*, 102(49), 10082–10089, doi:10.1021/jp982809s, 1998.
- 10 Rönkkö, T., Virtanen, A., Vaaraslahti, K., Keskinen, J., Pirjola, L. and Lappi, M.: Effect of dilution conditions and driving parameters on nucleation mode particles in diesel exhaust: Laboratory and on-road study, *Atmos. Environ.*, 40(16), 2893–2901, doi:10.1016/j.atmosenv.2006.01.002, 2006.
- Saleh, R., Donahue, N. M. and Robinson, A. L.: Time Scales for Gas-Particle Partitioning Equilibration of Secondary Organic Aerosol Formed from Alpha-Pinene Ozonolysis, 2013.
- 15 Seinfeld, J. H. and Pandis, S. N.: Atmospheric chemistry and physics: from air pollution to climate change, Wiley., 1998.
- Sihto, S.-L., Kulmala, M., Kerminen, V.-M., Dal Maso, M., Petäjä, T., Riipinen, I., Korhonen, H., Arnold, F., Janson, R., Boy, M., Laaksonen, A. and Lehtinen, K. E. J.: Atmospheric sulphuric acid and aerosol formation: implications from atmospheric measurements for nucleation and early growth mechanisms, *Atmos. Chem. Phys.*, 6(12), 4079–4091, doi:10.5194/acp-6-4079-2006, 2006.
- 20 Timonen, H., Karjalainen, P., Saukko, E., Saarikoski, S., Aakko-Saksa, P., Simonen, P., Murtonen, T., Dal Maso, M., Kuuluvainen, H., Ahlberg, E., Svenningsson, B., Pagels, J., Brune, W. H., Keskinen, J., Worsnop, D. R., Hillamo, R. and Rönkkö, T.: Influence of fuel ethanol content on primary emissions and secondary aerosol formation potential for a modern flex-fuel gasoline vehicle, *Atmos. Chem. Phys. Discuss.*, (September), 1–28, doi:10.5194/acp-2016-579, 2016.
- 25 Tkacik, D. S., Lambe, A. T., Jathar, S., Li, X., Presto, A. A., Zhao, Y., Blake, D., Meinardi, S., Jayne, J. T., Croteau, P. L. and Robinson, A. L.: Secondary organic aerosol formation from in-use motor vehicle emissions using a potential aerosol mass reactor., *Environ. Sci. Technol.*, 48(19), 11235–42, doi:10.1021/es502239v, 2014.
- Volkamer, R., Jimenez, J. L., San Martini, F., Dzepina, K., Zhang, Q., Salcedo, D., Molina, L. T., Worsnop, D. R. and Molina, M. J.: Secondary organic aerosol formation from anthropogenic air pollution: Rapid and higher than expected, *Geophys. Res. Lett.*, 33(17), L17811, doi:10.1029/2006GL026899, 2006.
- 30 Wang, J., Jin, L., Gao, J., Shi, J., Zhao, Y., Liu, S., Jin, T., Bai, Z. and Wu, C. Y.: Investigation of speciated VOC in gasoline vehicular exhaust under ECE and EUDC test cycles, *Sci. Total Environ.*, 445–446, 110–116, doi:10.1016/j.scitotenv.2012.12.044, 2013.

35

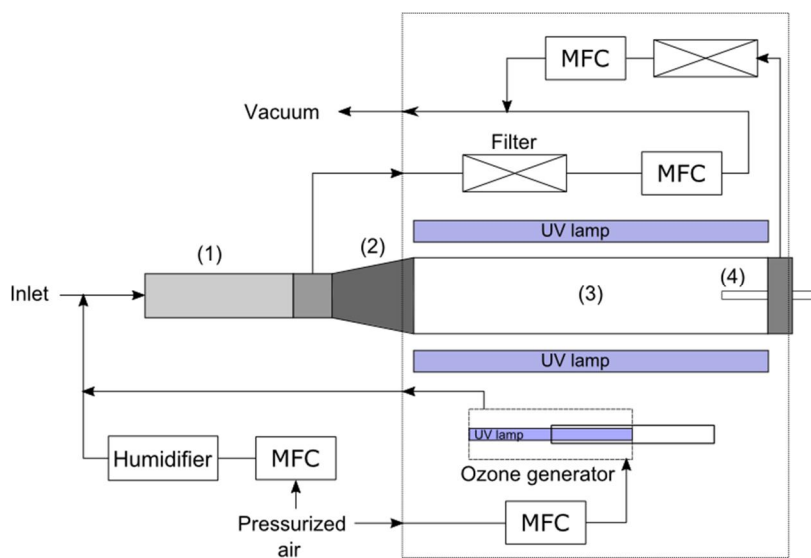
40

**Table 1: Toluene injection cycles**

Cycle 1		Cycle 2	
Time (s)	Injection	Time (s)	Injection
0	on	0	on
10	off	5	off
20	on	45	on
25	off	55	off
40	on	105	on
50	off	115	off

**Table 2. Dot product between the organic spectra of PAM and TSAR generated SOA.**

TSAR \ PAM	TSAR		
	Low oxidation	Medium oxidation	High oxidation
Low oxidation	0.999	0.904	0.779
Medium oxidation	0.904	0.999	0.978
High oxidation	0.773	0.962	0.999



5

**Figure 1. TSAR layout. The residence time chamber (1), the expansion tube (2), the oxidation reactor (3) and the adjustable outlet (4).**

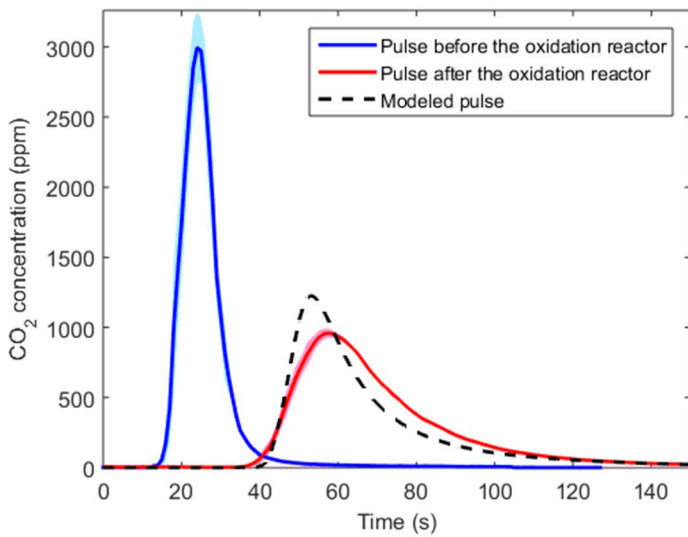
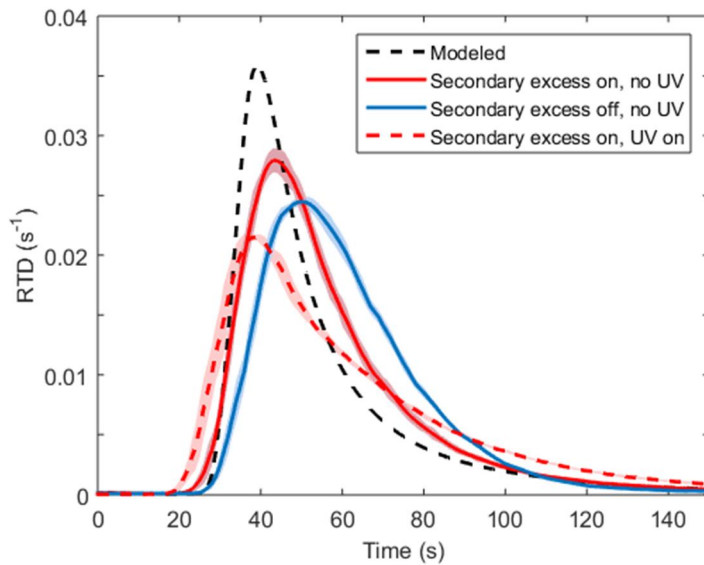


Figure 2. Measured and modeled  $\text{CO}_2$  pulses before and after the oxidation reactor. The shaded area shows the standard deviation of three pulses. The  $\text{CO}_2$  background of 380 ppm is subtracted from the results.



5 Figure 3. Modeled and measured residence time distributions with and without secondary excess flow and UV lights. The shaded area shows the standard deviation of three pulses.

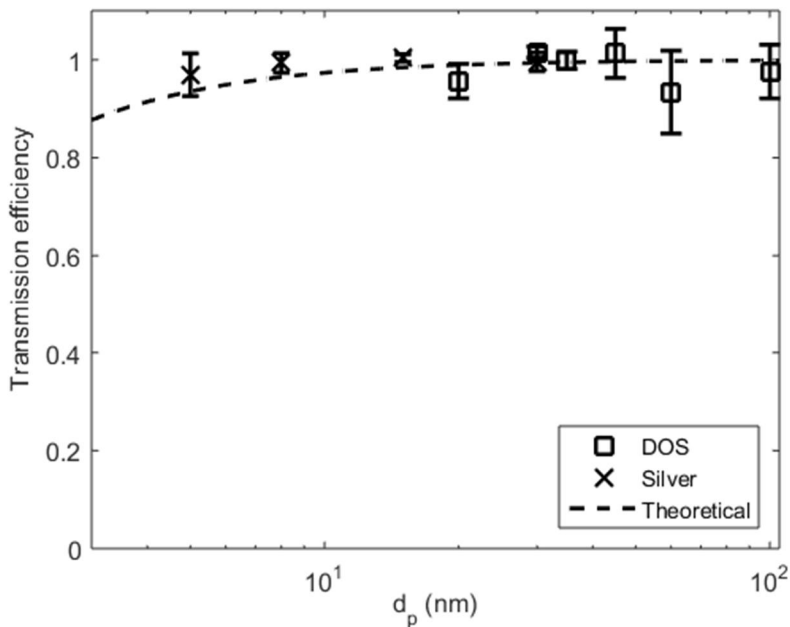


Figure 4. The particle transmission efficiency in TSAR oxidation reactor. The dashed line shows the theoretical transmission efficiency when the diffusion losses are taken into account. Error bars show the standard deviation.

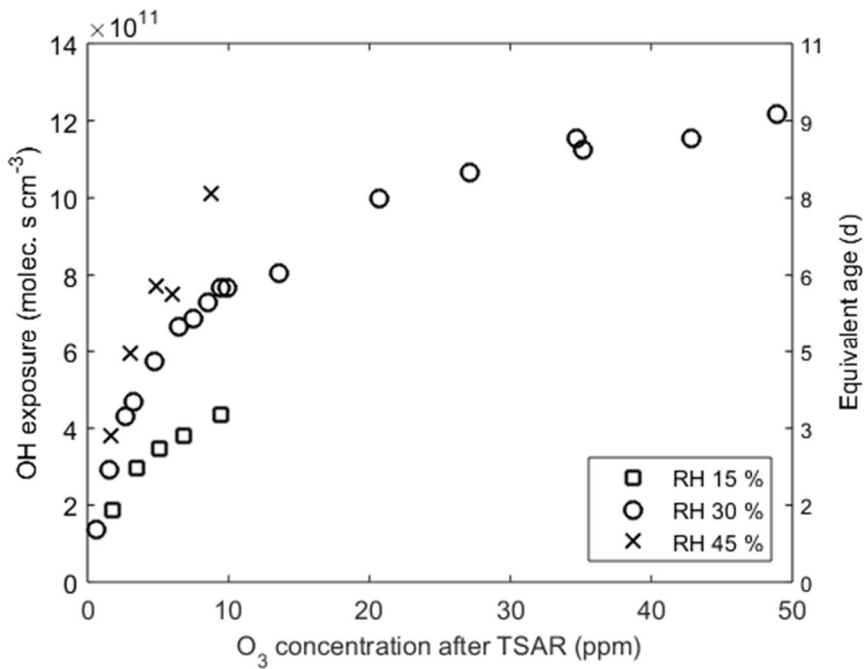


Figure 5. The OH exposure as a function of O<sub>3</sub> concentration after TSAR.

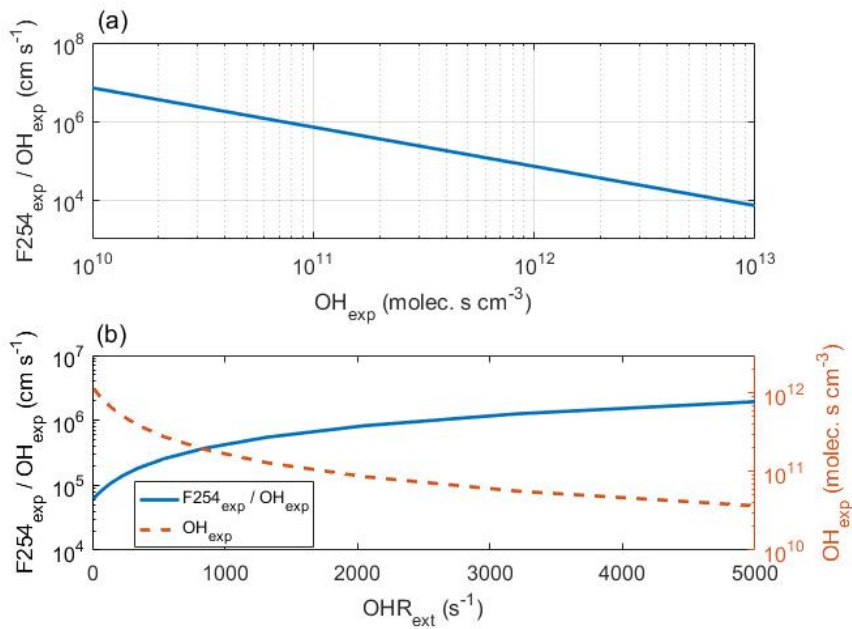
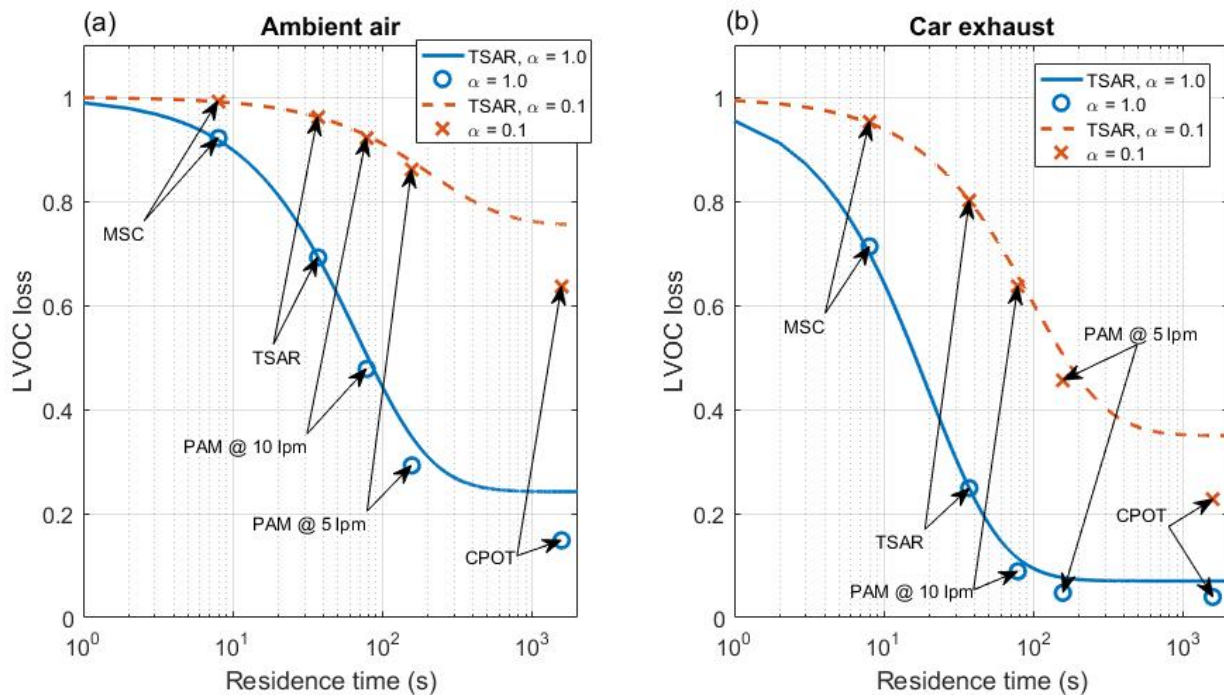


Figure 6. The ratio of 254 nm photon flux to OH exposure as a function of OH exposure (a) and external OH reactivity, when the initial ozone concentration is 45 ppm, relative humidity 30 % and temperature 20 °C (b). In (b), also the OH exposure dependence on OH reactivity is shown at same conditions.



**Figure 7. Modeled losses of low-volatile organic compounds as a function of residence time in TSAR in ambient case (a) and vehicle exhaust measurement (b) using two values for the accommodation coefficient ( $\alpha$ ). The model results for other flow reactors are also shown using typical residence times.**

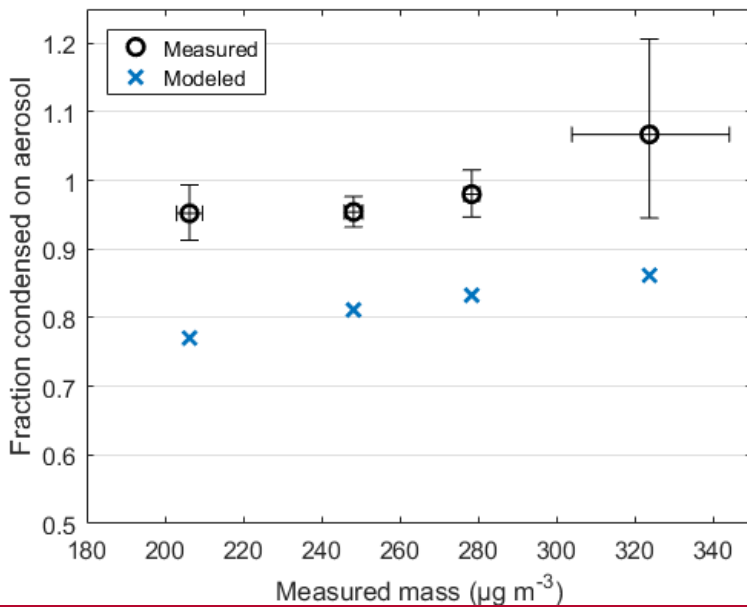
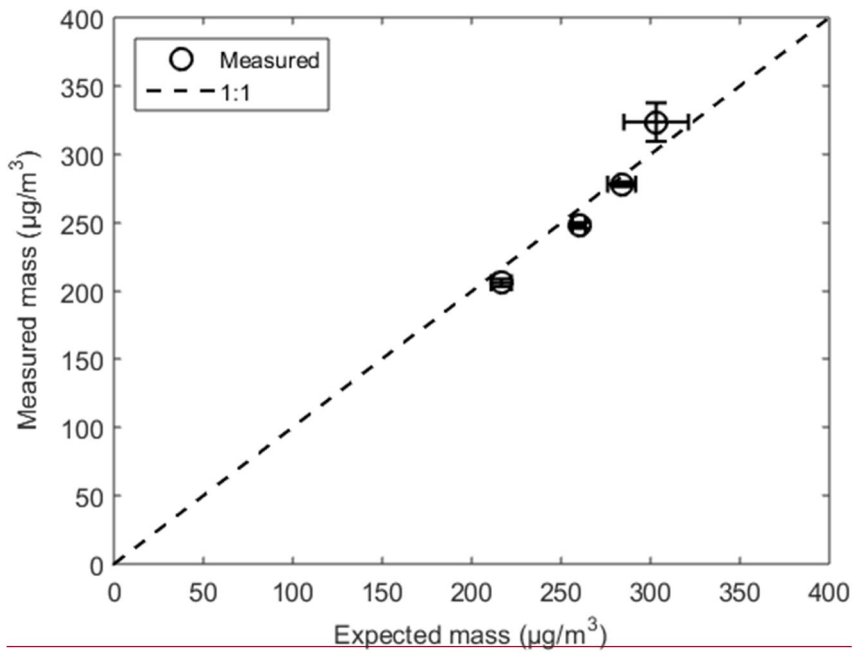


Figure 86. ~~Measured~~The fraction of the sulfuric acid mass condensed on aerosol phase as a function of ~~expected-measured~~ sulfuric acid mass.

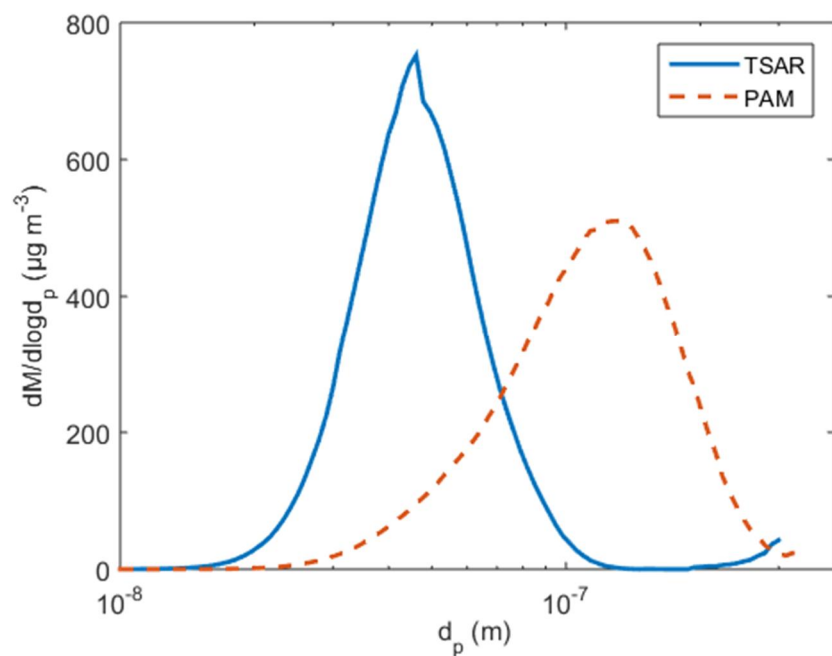


Figure 97. Particle mass size distributions for TSAR and PAM generated toluene SOA, obtained from SMPS particle number size distribution assuming spherical particles with a density of  $1.45 \text{ g cm}^{-3}$ .

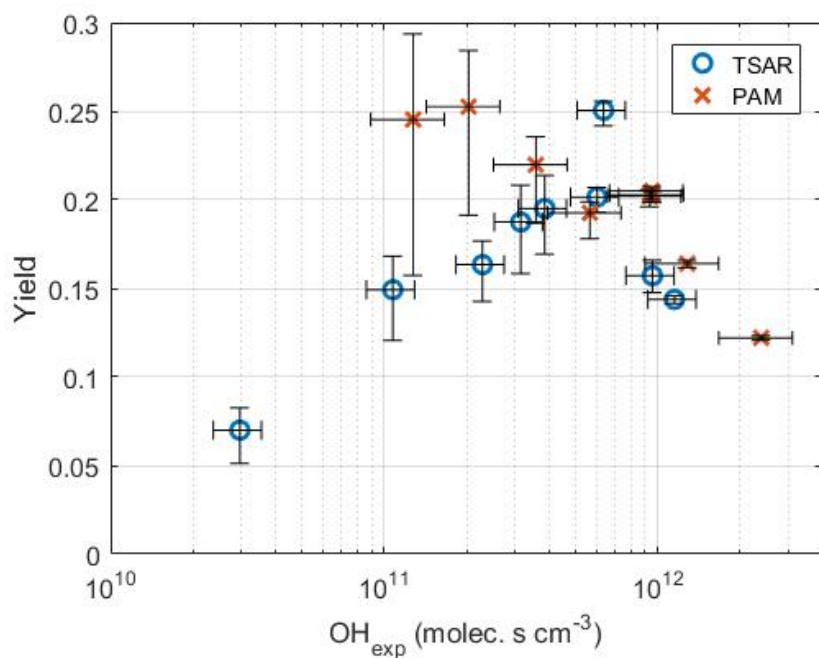
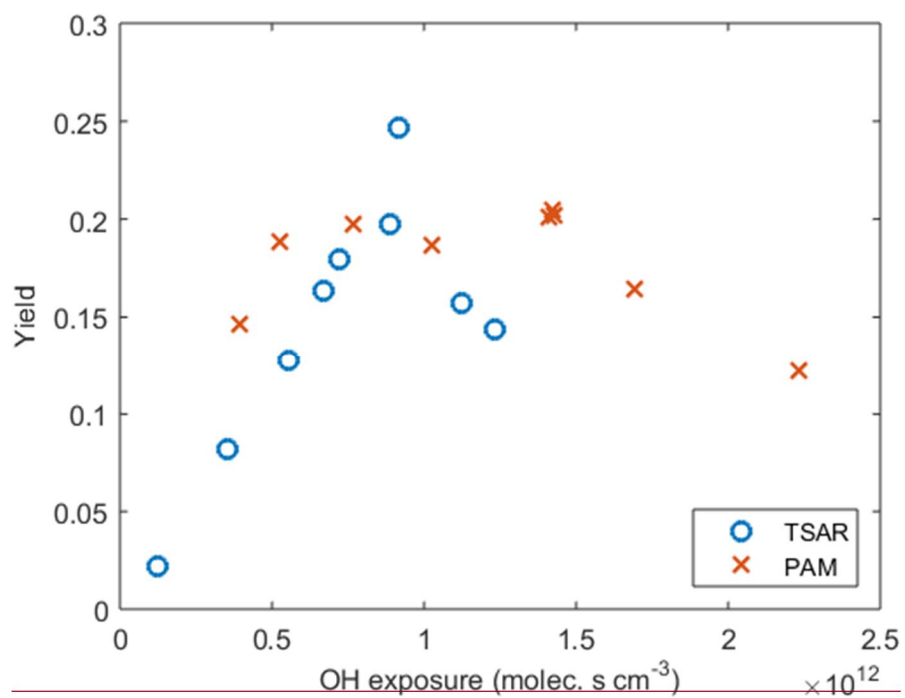


Figure 108. Toluene SOA yield as a function of OH exposure for both reactors.

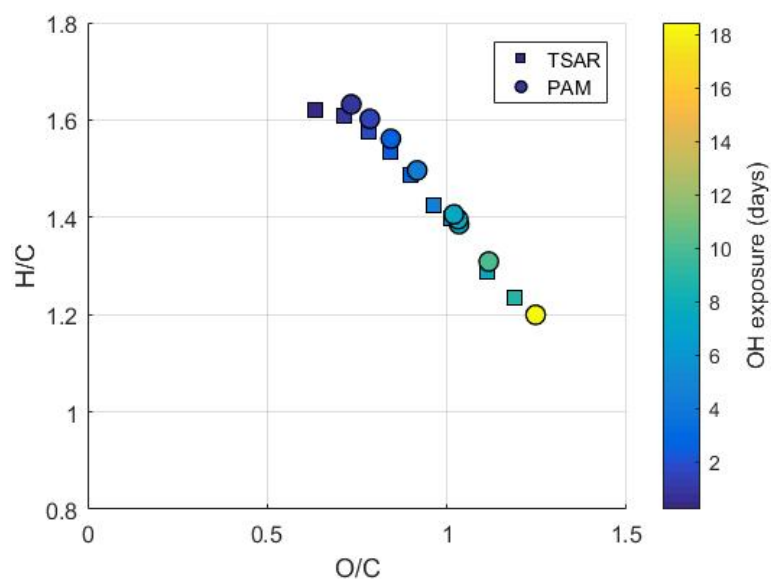
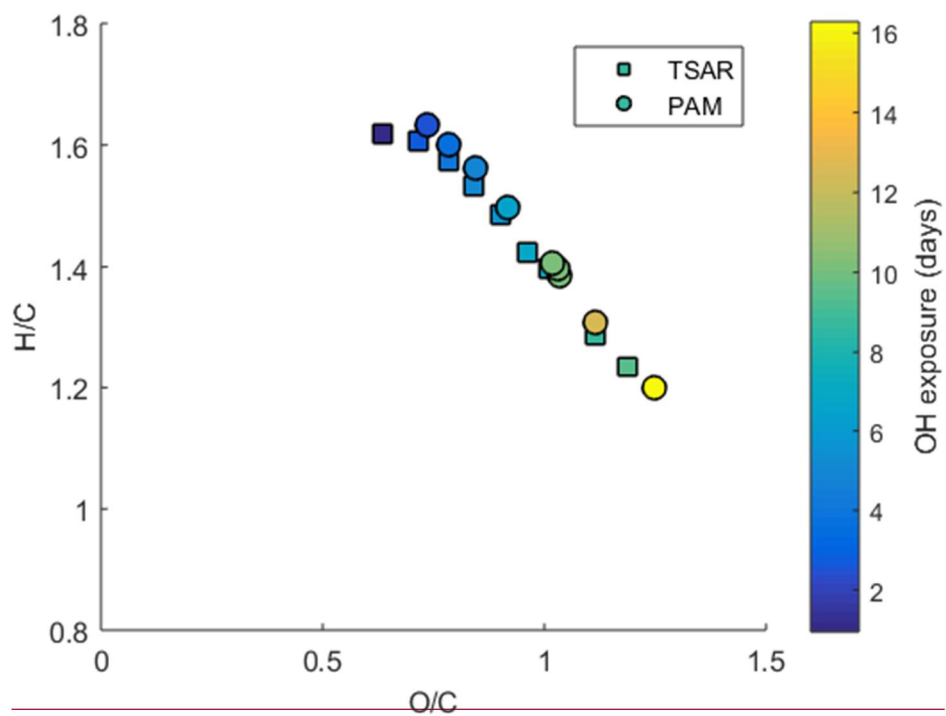


Figure 119. The van Krevelen diagram of toluene SOA for both chambers. The color indicates the OH exposure.

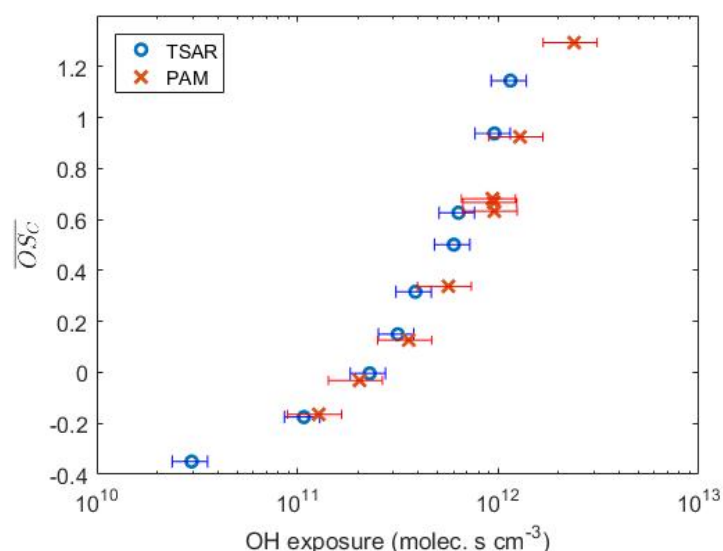
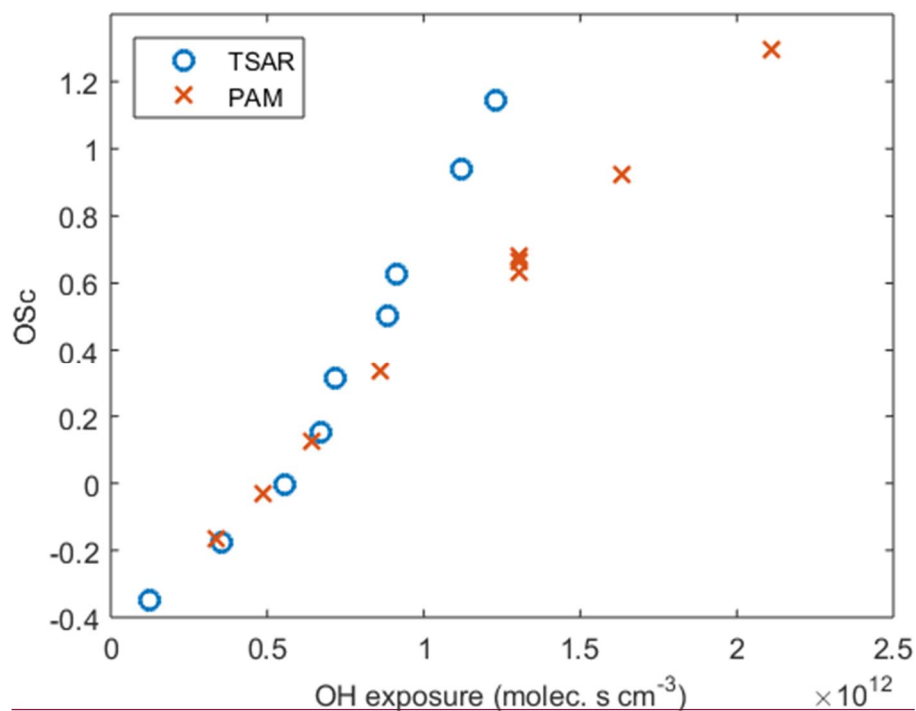
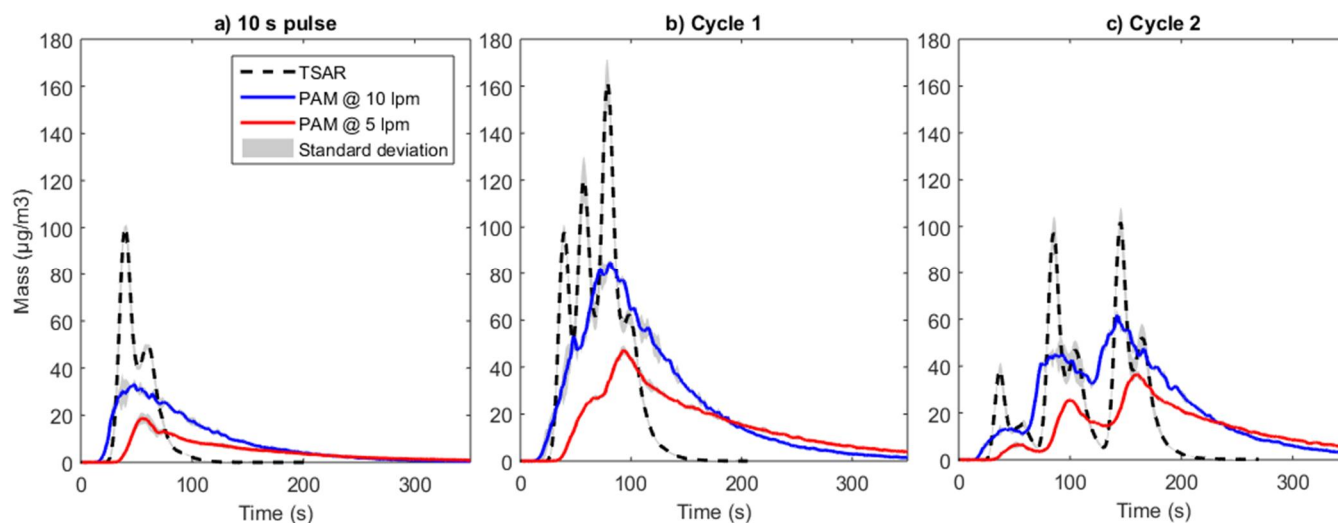


Figure 1240. The average carbon oxidation state ( $OSc$ ) as a function of OH exposure for PAM and TSAR generated toluene SOA.



5 Figure 1314. The mass produced from SOA formation of toluene pulses in TSAR at 5 slpm flow rate and in PAM at 5 and 10 slpm flow rates. The shaded area shows the standard deviation. The figures show the mass formation of a single pulse (a), cycle 1 (b) and cycle 2 (c), which both comprise of three adjacent pulses.

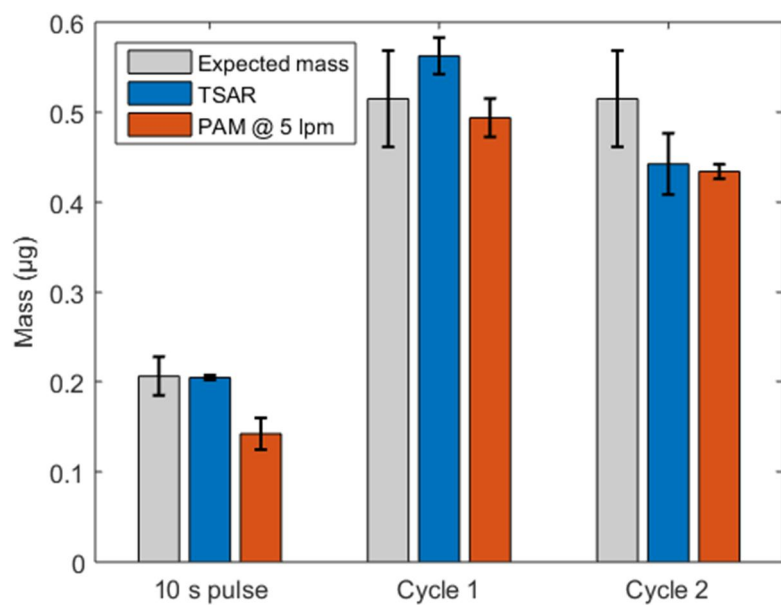
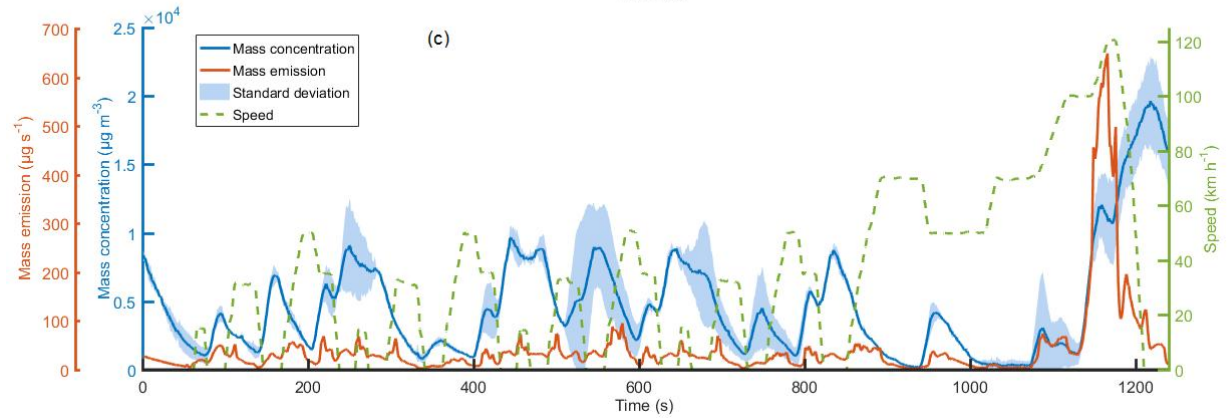
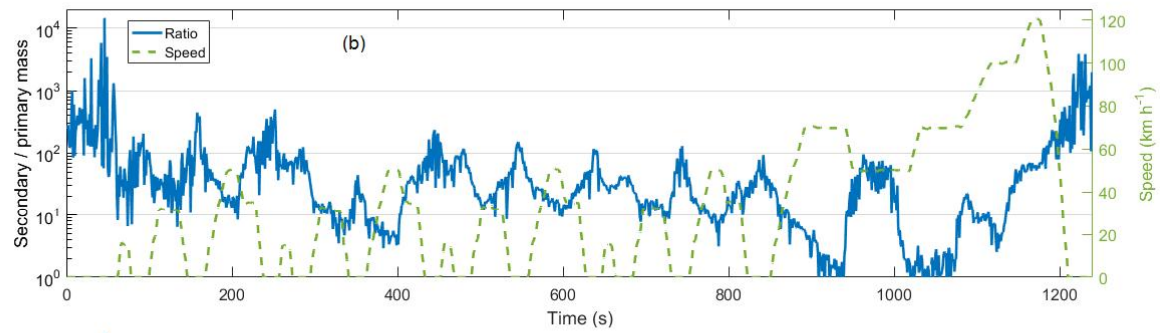
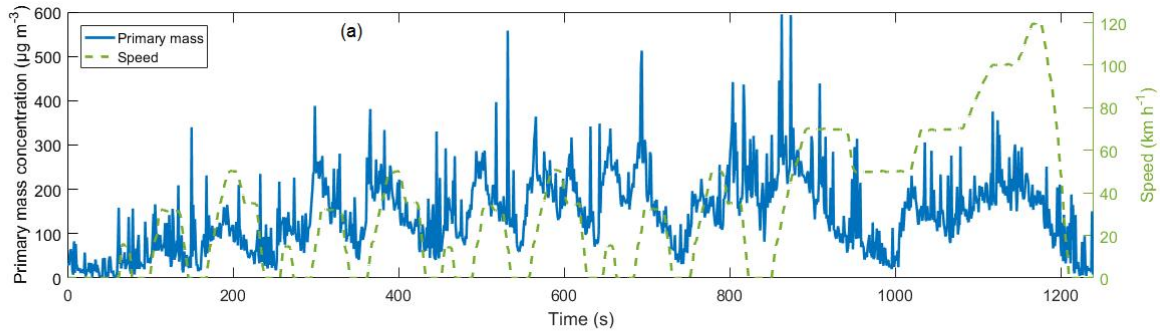
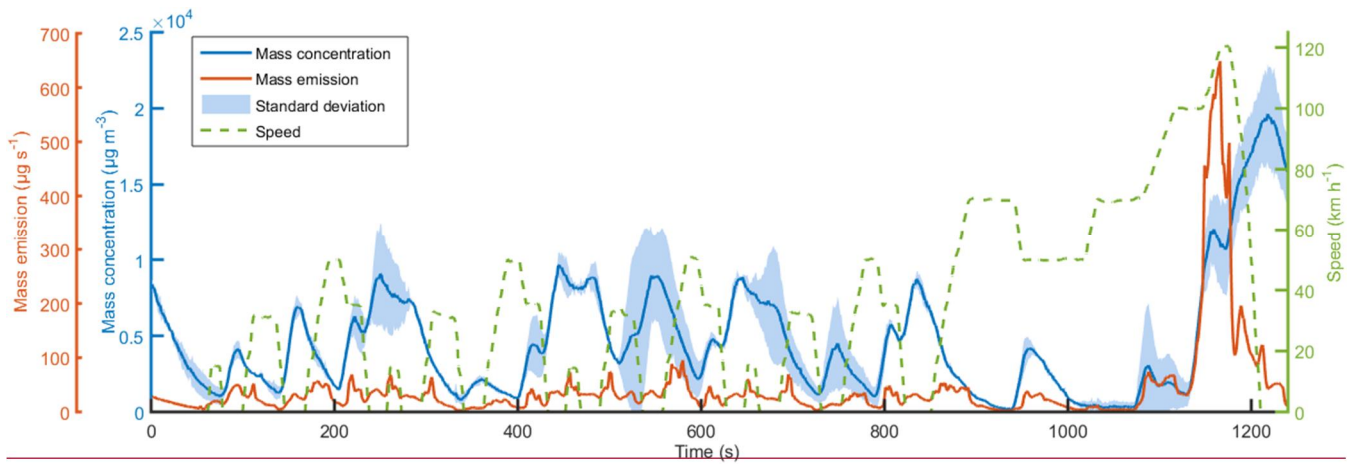


Figure 1412. The expected and measured masses produced in pulse experiments. The expected mass is calculated from the mass of injected toluene and its SOA yield.

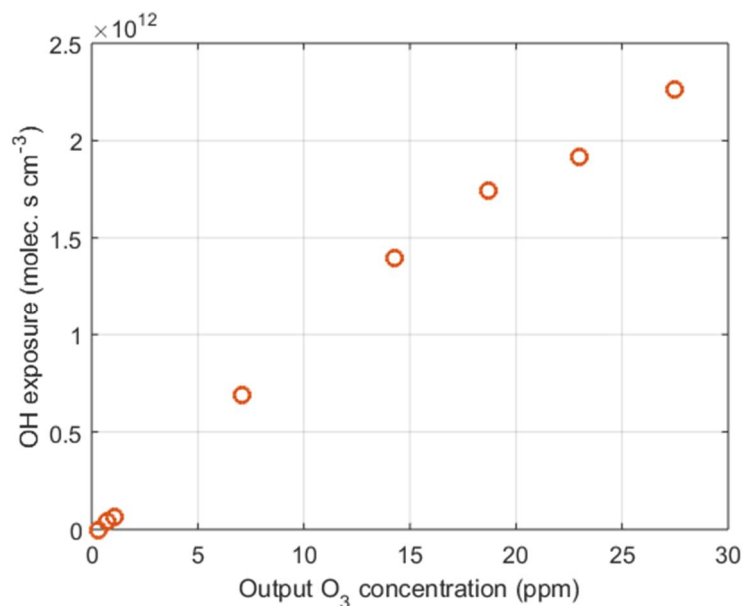


**Figure 1513.** Time-series of the vehicle speed and primary mass concentration (a), speed and the secondary-to-primary mass ratio (b), speed, the secondary mass concentration ( $\mu\text{g m}^{-3}$ ) and the secondary mass emission factor ( $\mu\text{g s}^{-1}$ ) (c) during the NEDC. The emission factor is obtained by multiplying the mass concentration by the total volumetric flow of the exhaust.

5

### Supplementary material

The PAM OH exposure as a function of ozone concentration measured after the PAM is presented in Fig. S1. The OH exposure was determined by measuring the SO<sub>2</sub> loss as in Sect. 2.4, and the different ozone concentrations are achieved by varying the lamp voltage.



5

**Figure S1. PAM OH exposure as a function of output ozone concentration at relative humidity of 27 – 29 %.**

Figure S2 shows the sampling setup for engine exhaust measurements. The primary dilution ratio is adjusted by the amount of dilution air for the porous tube diluter and by the flow rate to the vacuum after the residence time chamber.

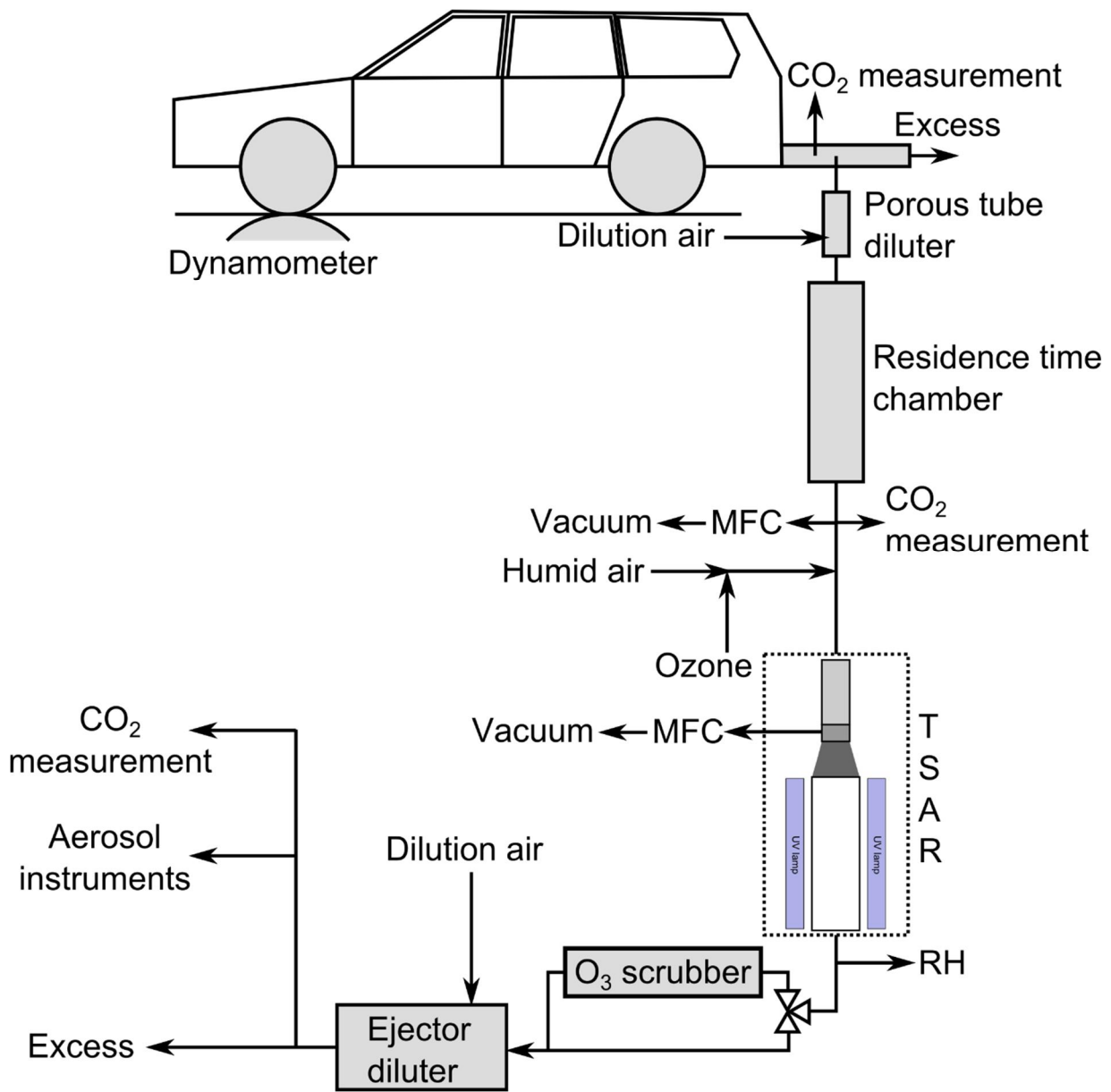


Figure S2. Engine exhaust sampling setup.

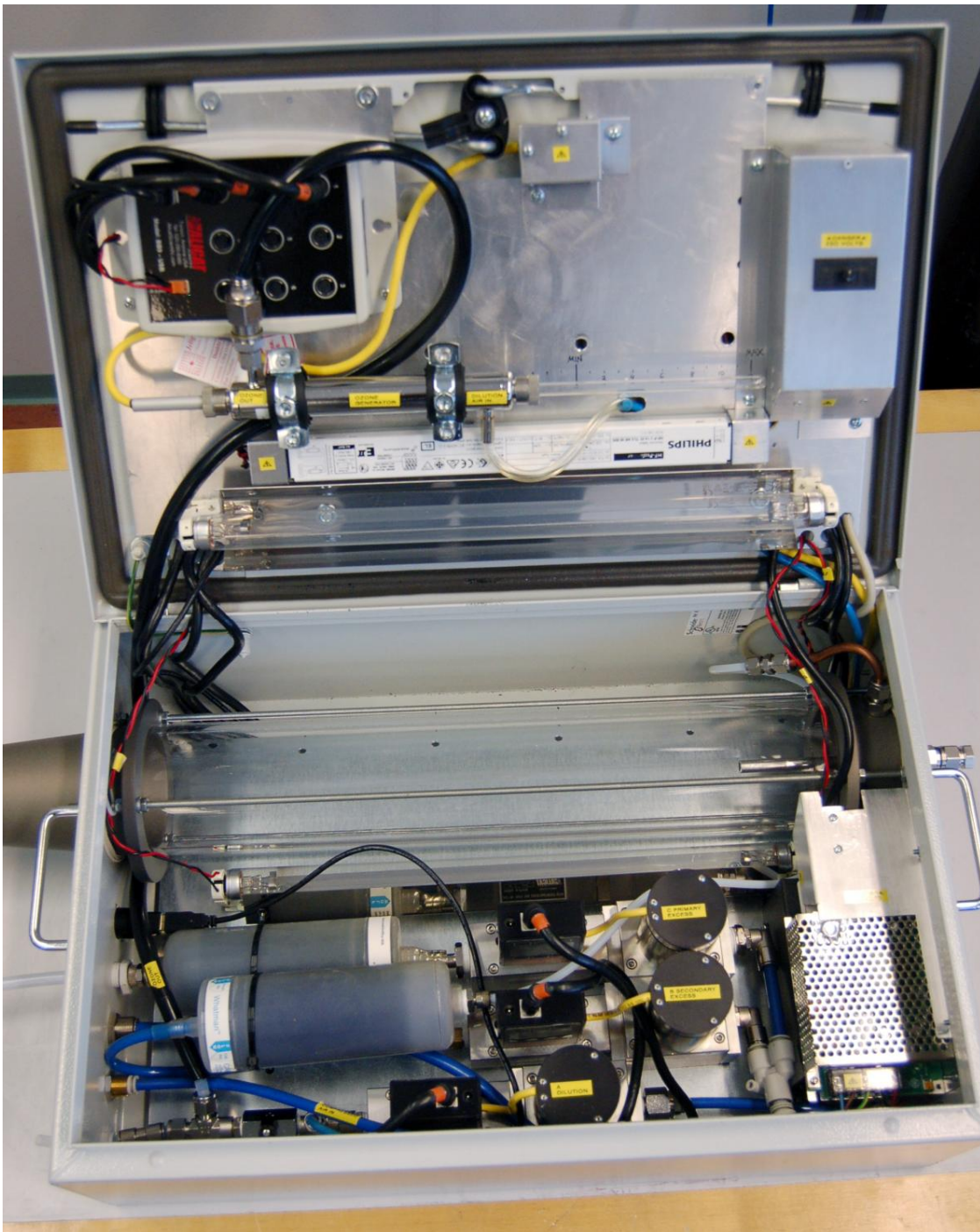
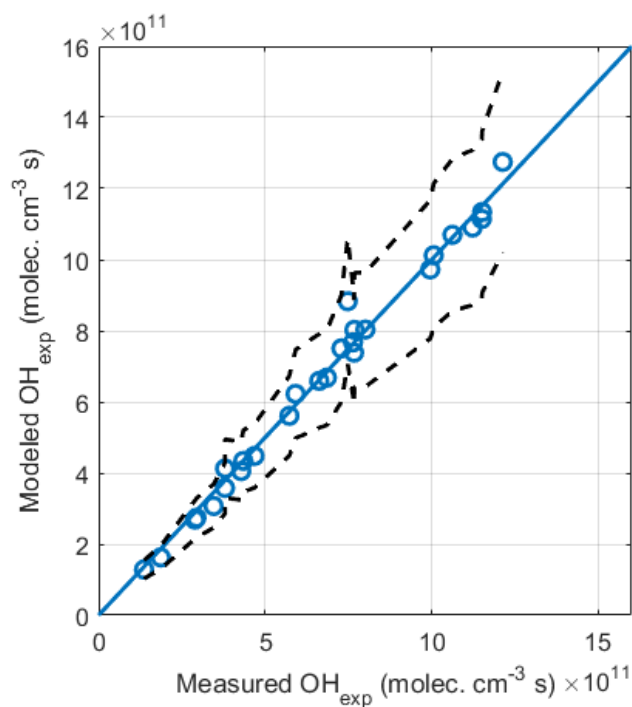
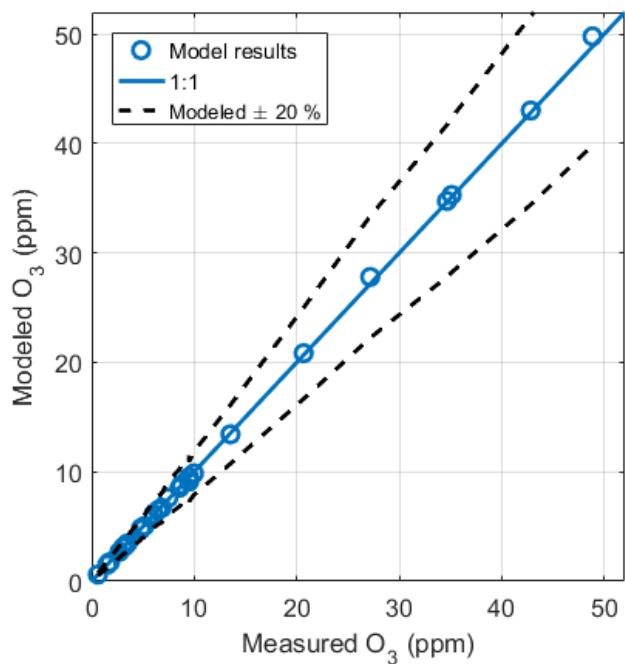
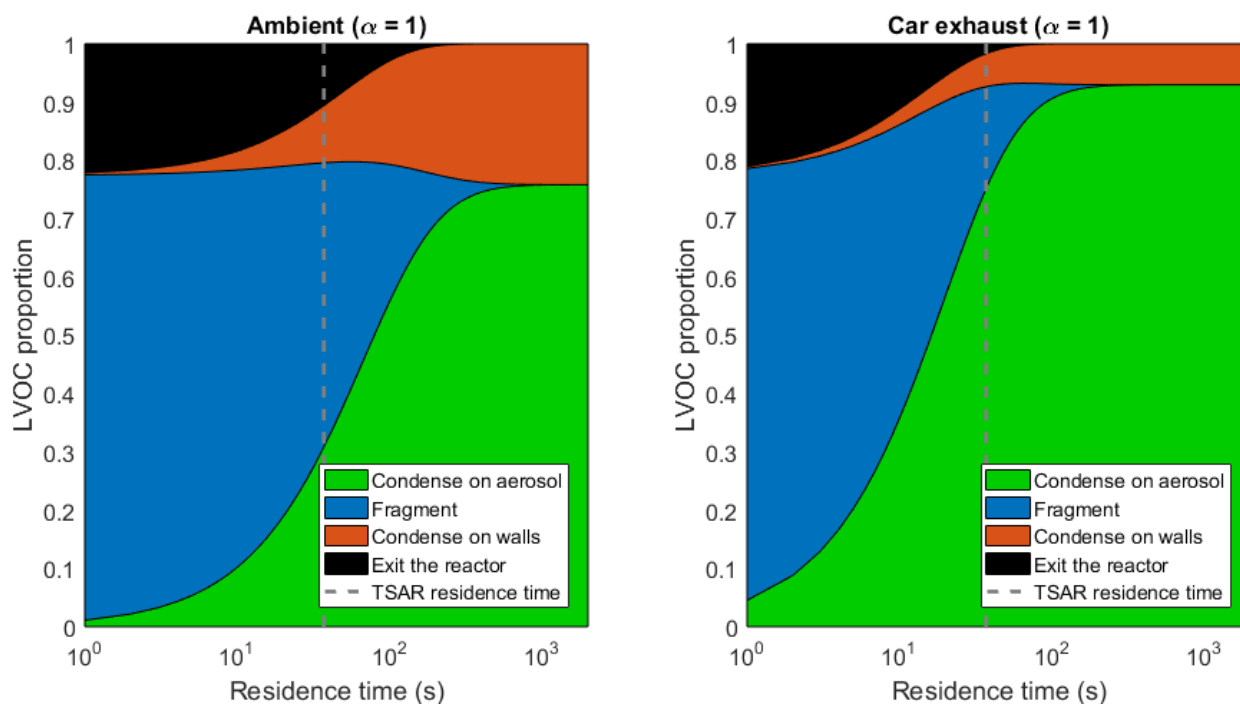


Figure S3. A photograph of TSAR



**Figure S4.** The measured and modeled ozone concentration after TSAR, and the measured and modeled OH exposure for the measurements done in Sect. 3.3.



**5** **Figure S5.** The fate of LVOC as a function of residence time for the ambient and the car exhaust case.

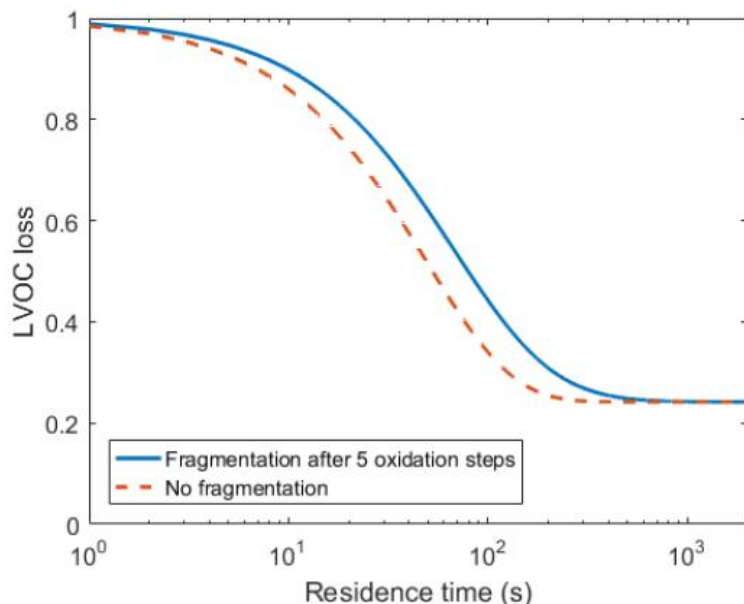
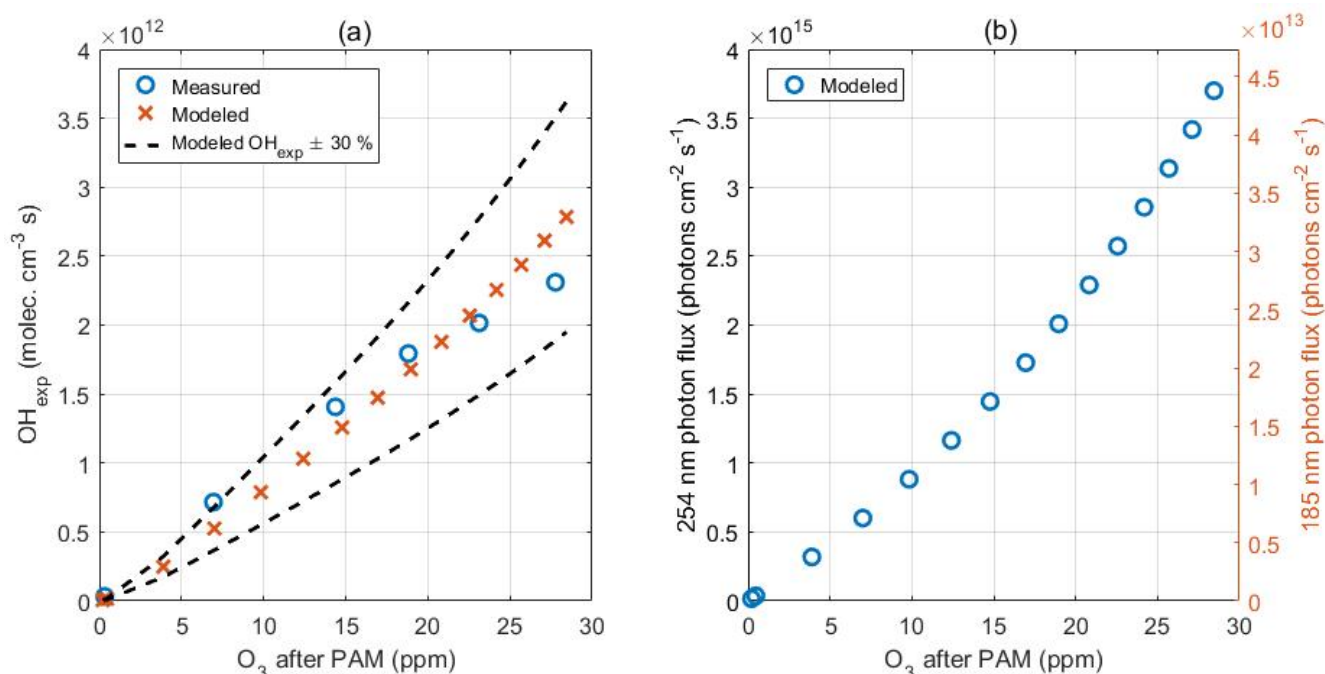


**Figure S6. The sensitivity of fragmentation parameter in LVOC loss model for the ambient case. If no fragmentation occurs, the losses are slightly lower at residence times between 10-300 s.**



**5 Figure S7. Comparison of model and measurement results of PAM OH exposure characterization (a), and the modeled photon flux as a function of modeled ozone concentration after PAM (b). The results were obtained by assuming OH wall loss coefficient of  $8.3 \text{ s}^{-1}$ , ozone wall loss coefficient of  $7.5 \times 10^{-4} \text{ s}^{-1}$  and that the 185 nm photon flux is 1.28 % of 254 nm photon flux. The input parameters were relative humidity, temperature, the initial  $\text{SO}_2$  concentration and the 254 nm photon flux.**

### Calculation of CS and $k_w$ in LVOC loss model

- 10 The condensational sink for a discrete particle size distribution is defined as

$$CS = \sum_i \beta(r_i) r_i N_i,$$

where  $r_i$  is the radius of particles in the  $i$ th size bin,  $N_i$  is the number concentration of particles and  $\beta$  is the transitional correction factor.

$$\beta = \frac{Kn + 1}{0.377Kn + 1 + \frac{4}{3\alpha}Kn^2 + \frac{4}{3\alpha}Kn},$$

where  $\alpha$  is the accommodation coefficient of condensing vapor.  $Kn$  is the Knudsen number.

$$Kn = 3 \sqrt{\frac{\pi m D}{8 k T r}}$$

where  $m$  is the molecular mass and  $D$  is the diffusion coefficient of the condensing vapor. (Pirjola et al., 1999)

5 The first-order wall loss rate coefficient is calculated with equation

$$k_w = \frac{2A}{\pi V} \sqrt{k_e D}$$

where  $A$  is the reactor surface area,  $V$  is the volume of the reactor,  $D$  is the diffusion coefficient of the condensing compound and  $k_e$  is the coefficient of eddy diffusion. (Palm et al., 2016) The reactor volume dependent value of  $k_e$  is calculated as in (Krechmer et al., 2016):

10 
$$k_e = 0.004 + (5.6 \times 10^{-3}) \cdot V^{0.74}$$

### References

- 15 Krechmer, J. E., Pagonis, D., Ziemann, P. J. and Jimenez, J. L.: Quantification of Gas-Wall Partitioning in Teflon Environmental Chambers Using Rapid Bursts of Low-Volatility Oxidized Species Generated in Situ, Environ. Sci. Technol., 50(11), 5757–5765, doi:10.1021/acs.est.6b00606, 2016.
- Palm, B. B., Campuzano-Jost, P., Ortega, A. M., Day, D. A., Kaser, L., Jud, W., Karl, T., Hansel, A., Hunter, J. F., Cross, E. S., Kroll, J. H., Peng, Z., Brune, W. H. and Jimenez, J. L.: In situ secondary organic aerosol formation from ambient pine forest air using an oxidation flow reactor, Atmos. Chem. Phys., 16(5), 2943–2970, doi:10.5194/acp-16-2943-2016, 2016.
- 20 Pirjola, L., Kulmala, M., Wilck, R. M., S, S. A. B., S, F. S. and A, E. O.: Formation of Sulphuric Acid Aerosols and Cloud Condensation Nuclei : an Expression for Significant Nucleation and Model Comparison, , 30(8), 1079–1094, 1999.